Marine Chemistry 220 (2020) 103750

Contents lists available at ScienceDirect

Marine Chemistry

journal homepage: www.elsevier.com/locate/marchem

Variations in sediment production of dissolved iron across a continental margin not dominated by major upwelling or riverine inputs

Eryn M. Eitel[a,*,1], Shannon M. Owings[a], Keaton M. Belli[a], Jordon S. Beckler[a,b], Anna Williams[a], Benjamin P. Fields[a], Malory Brown[a], Joel Craig[a], Olivia Bailey Studebaker[a], Donald B. Nuzzio[c], Martial Taillefert[a]

[a] School of Earth and Atmospheric Sciences, Georgia Institute of Technology, Atlanta, GA 30332, United States of America
[b] Harbor Branch Oceanographic Institute, Florida Atlantic University, Fort Pierce, FL 34946, United States of America
[c] Analytical Instrument Systems, Inc, Ringoes, NJ 08551, United States of America

A B S T R A C T

Despite the undeniable effect of iron on shaping patterns of ocean productivity, the relative importance of the different sources of this limiting nutrient to the ocean is still under debate. Although global estimates indicate that the benthic input of iron to the oceans is significant, most studies have investigated continental margins exposed to either upwelling or large riverine inputs, environments that are not representative of the majority of the oceans. Additionally, the number of studies that report dissolved iron concentrations in continental slope sediments is limited, despite the fact that these regions between the shelf edge and the continental rise make up >5% of the sedimentary surface area of the global ocean. The sedimentary flux of iron has traditionally been considered negligible due to the rapid oxidation of Fe^{2+} in oxic waters and poor solubility of the Fe(III) product. The recent realization that ferric iron may be stabilized in solution by organic ligands during oxidation near the sediment-water interface suggests that a significant fraction of the dissolved iron pool may be present under the form organic-Fe(III) complexes that could eventually reach the overlying waters. In this study, the speciation and biogeochemical importance of iron was determined in intact sediment cores along a transect across the entire continental margin near Cape Lookout, North Carolina, a region not dominated by upwelling or riverine inputs that is representative of most passive continental margins. Rates of diffusive oxygen uptake (DOU) and maximum diffusive fluxes of both dissolved Fe^{2+} and organic-Fe(III) complexes decreased from the coastal zone to the continental shelf, remained low on the shelf and the upper continental slope, but rebounded to reach a maximum in mid-slope sediments where concentrations of Fe(III) oxides were the highest along the transect. In turn, DOU decreased and dissolved iron was below detection in lower-slope sediments, indicating that mid-slope sediments represent depocenters where Fe(III) oxides and organic matter may accumulate. Pore water sulfate and sulfide concentrations as well as separate sediment incubations confirmed that sulfate reduction does not greatly influence the cycling of iron in these sediments. The production of dissolved organic-Fe(III) in these continental margin sediments is likely regulated by a combination of aerobic oxidation in the presence of natural organic ligands near the sediment-water interface, dissimilatory iron reduction, or chemical oxidation of Fe(II) complexed to natural organic ligands. Fluxes of Fe^{2+} and organic-Fe(III) complexes across the sediment-water interface were not observed. However, diffusive fluxes of Fe^{2+} and organic-Fe(III) complexes into the oxic zone of these sediments (<1 cm from the sediment-water interface) and production of dissolved Fe(III) in sediment slurry incubations suggest that complexation of Fe(III) in these sediments may contribute to the stabilization and potential transport of dissolved iron into oxygenated deep ocean waters. Extrapolation to the global ocean suggests that mid-slope depocenters contribute considerably to the iron inventory of the ocean, thus warranting the need for measurement of benthic iron fluxes and dissolved iron speciation in these environments.

1. Introduction

Iron exerts substantial control on ocean productivity and the export of organic matter to the deep ocean with potentially large-scale feedbacks within the global climate system (Falkowski et al., 1998; Jickells et al., 2005; Martin, 1990). As iron is an essential nutrient for phytoplankton, low concentrations may limit primary productivity in a large portion of the world's oceans including high-nutrient, low-chlorophyll (HNLC) regions (Coale et al., 1996; Kolber et al., 1994; Martin and Fitzwater, 1988), the low-nutrient South Pacific gyre (Behrenfeld and Kolber, 1999), and the Southern Ocean (de Baar et al., 1990). By providing a flux of 1–6 × 10^{11} mol Fe yr^{-1} (Fung et al., 2000; Jickells and Spokes, 2001), wind driven, atmospheric inputs of land-derived particulate iron is a major source of iron to the open ocean, despite its limited solubility in seawater (1–10%) (Jickells and Spokes, 2001; Jickells et al., 2005; Johnson et al., 1997). However, large areas of the Antarctic and Southern Pacific Oceans receive low atmospheric iron inputs (Honjo et al., 2000) such that alternative iron sources are

* Corresponding author at: School of Earth and Atmospheric Sciences, Georgia Institute of Technology, Atlanta, GA 30332, United States of America.
E-mail address: eeitel@caltech.edu (E.M. Eitel).
[1] Present address: Geological and Planetary Science, California Institute of Technology, Pasadena, CA 91125, United States of America

https://doi.org/10.1016/j.marchem.2020.103750

Available online 09 January 2020

required to account for the observed biological activity in these regions (Moore et al., 2002). Icebergs and glacial meltwater contribute comparable amounts of bioavailable iron as aeolian dust in a limited number of polar regions (Bhatia et al., 2013; Raiswell et al., 2008), and hydrothermal vents may also sustain primary production even when atmospheric inputs are limited by generating an estimated dissolved iron flux of 0.9×10^9 mol Fe yr^{-1} (Tagliabue et al., 2010). Riverine sources are estimated to provide $1.5–26 \times 10^9$ mol Fe yr^{-1} based on the average concentration of dissolved iron (40 nM Fe) in the major world rivers (Martin and Meybeck, 1979; Poulton and Raiswell, 2002). However, the effective riverine input to the oceans may be reduced up to 90% due to flocculation and precipitation during estuarine mixing (Boyle et al., 1977). Continental shelf sediment re-mobilization and lateral advection may provide a source of particulate iron to the ocean (Chase et al., 2005; Johnson et al., 1999) and HNLC zones (Lam and Bishop, 2008; Lam et al., 2006), and dissolved iron diffusing out of margin sediments may be transported to surface waters in upwelling zones (Bruland et al., 2001; Coale et al., 1996; Elrod et al., 2004). Overall, benthic dissolved iron fluxes to the euphotic zone based on carbon oxidation rates and bottom water O_2 is predicted to be 72×10^9 mol Fe yr^{-1} from shelf sediments (<200 m) and 37×10^9 mol Fe yr^{-1} from slope sediments (200–2000 m) (Dale et al., 2015). However, such global estimates of continental margin input may currently be biased due to the number of studies investigating zones of intense upwelling and the limited characterization of iron speciation in these studies.

Little dissolved iron is available in the oceans due to the rapid oxidation of Fe^{2+} in fully oxygenated waters (Millero et al., 1995) and low solubility of Fe(III) at circumneutral pH (Liu and Millero, 2002). However, ferric iron is stabilized in seawater by complexation with Fe (III)-binding ligands (Millero, 1998; Taillefert et al., 2000a; Wu et al., 2001). In fact, >90% of dissolved Fe(III) in open ocean and coastal waters is complexed by strong organic Fe-binding ligands (Gledhill and Van Den Berg, 1994; Rue and Bruland, 1995; Rue and Bruland, 1997; van den Berg, 1995; Wu and Luther, 1994). Dissolved Fe is stabilized by dissolved organic matter (DOM) from both riverine (Gerringa et al., 2007; Perdue et al., 1976) and sedimentary (Burdige et al., 1992; Jones et al., 2011) origin, biologically-produced siderophores (Macrellis et al., 2001), and phytoplankton exudates (Chen et al., 2004), although strong L_1-type ligands not correlated with chlorophyll have been observed to dictate the concentration of dissolved Fe in river plume, estuarine, and upwelled surface waters (Buck et al., 2007; Jones et al., 2011). In continental margin sediments, observation of dissolved Fe(III) and Fe^{2+} at similar concentrations along with decreased oxidation of Fe^{2+} and removal as Fe(III) oxyhydroxide (Lohan and Bruland, 2008; Severmann et al., 2010) suggests iron is stabilized in solution by complexation. Stabilization of Fe(III) by complexation in sediments increases iron bioavailability (Chase et al., 2005) and may significantly impact the offshore transport of dissolved iron of sedimentary origin (Buck et al., 2007; Chase et al., 2005; Jones et al., 2011).

Most studies of benthic iron input to the oceans have been conducted in continental shelf sediments either associated with upwelling near HNLC regions (Berelson et al., 2003; Elrod et al., 2004; Esch et al., 2013; Lam and Bishop, 2008) or exposed to riverine inputs and seasonal hypoxia (Friedl et al., 1998; Friedrich et al., 2002; Lohan and Bruland, 2008; Noffke et al., 2012; Severmann et al., 2010). To our knowledge, iron reduction in continental margin sediments with limited upwelling or riverine input has never been measured. In addition, iron flux measurements in continental slope sediments are limited (Elrod et al., 2004; Noffke et al., 2012; Severmann et al., 2010) despite the fact that these regions between the shelf edge and the continental rise make up >5% of the oceans sedimentary surface area compared to <9% for continental shelf sediments (Harris et al., 2014). Furthermore, iron speciation as well as the mechanism behind the production of dissolved iron in both shelf and slope sediments is not often investigated. Understanding whether dissolved iron produced in sediments is stabilized by complexation is important to assess the potential for continental margin sediments to release iron under a bioavailable form in oxic ocean waters. In this study, the continental shelf and slope near Cape Lookout, North Carolina was investigated to evaluate the potential for passive continental margin sediments without large upwelling events or riverine input to act as an iron source to the ocean. As the speciation of dissolved iron may greatly affect its residence time, both dissolved Fe^{2+} and organic-Fe(III) complexes (org-Fe(III) were measured, and the underlying biogeochemical processes affecting iron production and upward diffusive flux in these sediments were investigated.

2. Methods

2.1. Site description and sediment sampling

Sediment cores were obtained from the continental slope near Cape Lookout, North Carolina using either a single corer (Marinelli et al., 1998) or a MC-800 multicorer (Ocean Instruments, Inc.) during cruises conducted in June 2010, June 2011, June 2012, July 2015, and May 2016 on the R\V Savannah. Sediments were sampled in the coastal zone (0–20 m), across the shelf (20–50 m), over the upper-slope (50–500 m), the mid-slope (500–900 m), and the lower-slope (900–1500 m) (Fig. 1, Table 1). As determined through both visual observations and in previous studies (Anderson et al., 1994; Blake et al., 1985; Milliman et al., 1972), the shelf is dominated by sand, however the proportion of silt and clay increases with water column depth from the upper- to lower-slope. Water column depth was determined along the transect between 34.6802 N 76.6469 W and 33.4706 N 75.5169 W using 1-minute ETOPO1 bathymetry (Amante and Eakins, 2009). To the south of Cape Lookout, the continental slope joins the Blake Ridge at about 32°30′N where the gradient of the slope averages 3.5°, whereas north of Cape Lookout near Cape Hatteras the slope gradient reaches a maximum of about 16° (Popenoe, 1980). The waters off the coast of North Carolina are primarily influenced by the Gulf Stream and the Western Boundary Undercurrent (WBUC). The WBUC flows southwest from the Labrador Sea and crosses below the Gulf Stream axis at depth of 2000 m near Cape Hatteras (Barrett, 1965; Richardson, 1977). To the south off Cape Lookout, an upper boundary of 1000 m is suggested for the WBUC (Rowe and Menzies, 1968). The Gulf Stream flows along the continental margin northeast from Florida over the Blake Plateau to Cape Hatteras where it turns easterly towards the North Atlantic. Near Cape Lookout, the lower boundary of the Gulf Stream may be as shallow as 600 m (Pratt, 1966), and not deeper than 1000 m on the Carolina margin, indicating that it does not mix with the WBUC (Johnson, 1989; Richardson, 1977; Rowe and Menzies, 1968). Therefore, the WBUC may influence the lower-slope and continental rise sediment, whereas the Gulf Stream tends to influence the bottom of the upper-slope, and the mid-slope receives the least direct influence from either of these currents (Blake et al., 1987). The Virginia Current, which flows south along the continental shelf in the Mid-Atlantic Bight converges with the Gulf Stream near Cape Hatteras and may contribute to limited local upwelling and intrusion events on the shelf or slope break, though these effects decrease to the south, near Cape Lookout (Csanady and Hamilton, 1988; Janowitz and Pietrafesa, 1980; Pietrafesa et al., 1985).

Due to the divergence of the Gulf Stream, Cape Hatteras serves as an important oceanographic barrier separating the southern tropical waters from the northern temperate waters (Cerame-Vivas and Gray, 1966; Milliman et al., 1972; Stefánsson et al., 1971) and is characterized by high deposition rates of organic matter and sediment particles despite no direct riverine inputs, high productivity, and completely oxygenated bottom waters (Blair et al., 1994; Blake et al., 1987; Blake et al., 1985; DeMaster et al., 1994; DeMaster et al., 2002; Diaz et al., 1994; Schaff et al., 1992; Thomas et al., 2002). High upwelling, sedimentation rates, and benthic macrofauna densities on the slope off Cape Hatteras, however, indicate this environment is atypical of the rest of the Atlantic slope (Aller et al., 2002; Rhoads and Hecker, 1994).

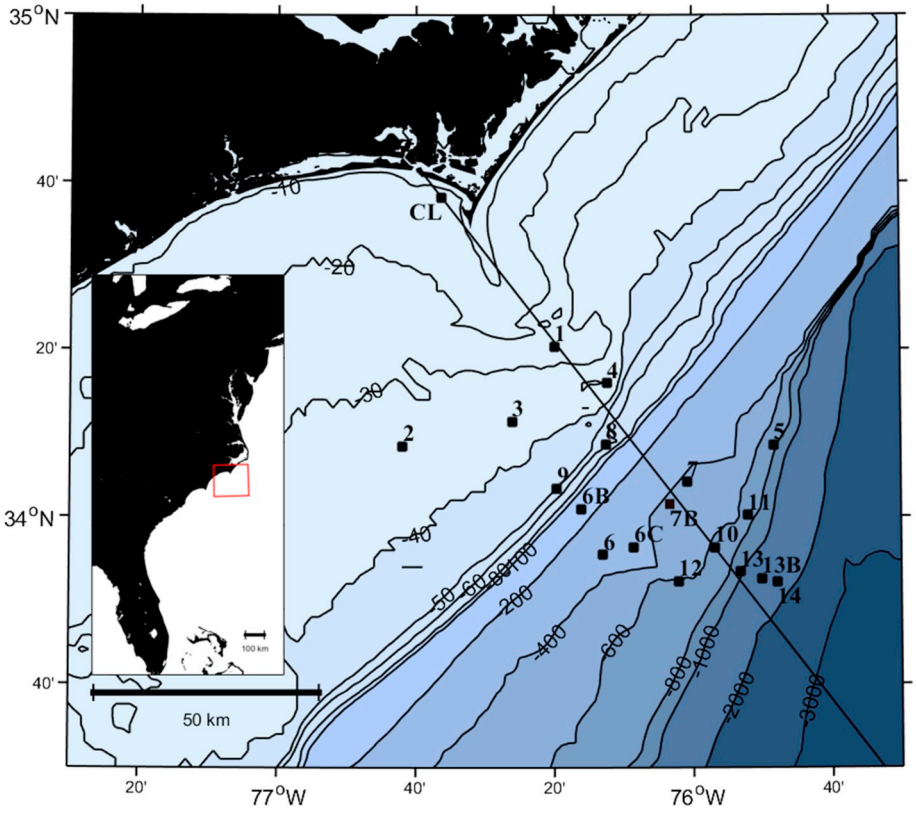

Fig. 1. Bathymetric map of the North Carolina continental margin near Cape Lookout with locations of the stations where sediment cores were collected between 2010 and 2016. The black line transect was used to represent characteristic continental margin bathymetry.

Table 1
Sediment core collection date, location, water depth, and bottom water temperature and salinity.

Station	Date	Long. (°W)	Lat. (°N)	Depth (m)	Temp (°C)	Salinity	O_2 (mM)
1	5/30/2010	−76.3326	34.3391	28.6	21.7	34	0.226
2	5/31/2010	−76.6986	34.1411	36.7	23.8	34.7	0.225
3	6/1/2010	−76.4348	34.1903	33.8	24.7	36	0.236
2	6/3/2010	−76.6845	34.1465	37.2	24.8	33	0.224
1	6/4/2010	−76.3260	34.3392	27.7	22.9	31.2	0.224
3	6/5/2010	−76.4335	34.1905	33.9	26.4	32	0.231
3	6/4/2011	−76.4318	34.1924	33.4	24.8	35.5	0.223
1	6/9/2011	−76.3339	34.3386	28.3	21.1	35.75	0.223
3	6/10/2011	−76.4343	34.1913	31.4	23.3	38	0.213
2	6/13/2011	−76.6963	34.1408	28.2	23.4	35	0.213
4	6/11/2012	−76.2070	34.2660	44	23.7	37.5	0.220
1	6/13/2012	−76.3326	34.3391	22.3	24.5	36	0.209
CL	6/14/2012	−76.5952	34.6363	13.6	24.7	35.3	0.213
CL	6/16/2012	−76.6050	34.6350	14.7	25.2	35	0.197
3	6/18/2012	−76.4343	34.1913	33.4	24.7	35.8	0.146
2	6/20/2012	−76.6845	34.1465	37	27.1	35	0.203
4	7/8/2015	−76.2070	34.2660	40	25	36	0.210
3	7/9/2015	−76.4343	34.1913	30	26	37	0.205
6B	7/11/2015	−76.2690	34.0160	150	22.5	39	0.217
7	7/12/2015	−76.0150	34.0690	423	15	37	0.229
6	7/12/2015	−76.2170	33.9240	290	19	37	0.220
6C	7/13/2015	−76.1420	33.9400	335	17	38	0.240
5	7/19/2015	−75.8060	34.1430	589	17	36	0.225
11	7/19/2015	−75.8700	34.0030	665	19	38	0.223
12	7/20/2015	−76.0348	33.8715	580	18	36	0.239
10	7/20/2015	−75.9560	33.9360	596	17	38	0.229
8	5/17/2016	−76.2100	34.1440	57	23.9	39	0.211
CL	5/18/2016	−76.6050	34.6350	14.7	20.2	37	0.242
7B	5/19/2016	−76.0580	34.0240	428	17.1	37	0.230
4	5/23/2016	−76.2070	34.2660	38	24.5	38	0.241
13	5/24/2016	−75.8870	33.8900	840	12.8	37	0.230
13B	5/24/2016	−75.8350	33.8770	1130	13.8	37	0.257
14	5/25/2016	−75.7990	33.8690	1450	12.4	37	0.254
9	5/26/2016	−76.3270	34.0570	63.7	25.2	40	0.210

Continental slope sediments to the south of Cape Hatteras at Cape Lookout and Cape Fear are not as thoroughly mixed (Schaff et al., 1992; DeMaster et al., 1994, Fornes et al., 1999) or as biologically active (Schaff et al., 1992; Blake and Grassle, 1994, Fornes et al., 1999, Aller et al., 2002, Gooday et al., 2001, Blake and Hilbig, 1994). In addition, the complex topography and numerous canyons, ridges, and gullies (McGregor, 1984; Mellor and Paull, 1994; Popenoe et al., 1982) make the Cape Hatteras sedimentary region difficult to study. As its sediment is more accessible and more representative of the Atlantic slope (Blake and Grassle, 1994), the sampling location near Cape Lookout was chosen instead. The continental margin off Cape Lookout includes comparable total organic carbon content to north or south locations in the upper 5 cm of slope sediment and is exposed to an intermediate sedimentation rate of 0.16 cm/yr (Blake et al., 1987; Schaff et al., 1992). Finally, relatively little evidence of downslope sliding has been observed by either submersibles or high resolution seismic profiles (DeMaster et al., 1994), and limited sulfate reduction has been detected (DeMaster et al., 1994; Schaff et al., 1992), indicating that dissimilatory iron reduction may represent a dominant anaerobic respiration process in these sediments.

2.2. Sediment and pore water analyses

Unless otherwise noted, all chemicals were of reagent grade or higher purity and obtained from Sigma-Aldrich. Depth profiles of dissolved O_2, Mn^{2+}, Fe^{2+}, total dissolved sulfide ($\Sigma H_2S = H_2S + HS^- + S(0) + S_x^{2-}$) as well as organic complexes of Fe(III) (org-Fe(III)) and iron sulfide clusters (FeS_{aq}) were obtained with mercury/gold amalgam (Hg/Au) voltammetric microelectrodes deployed in intact sediment cores using a micromanipulator within 30 min after collection. The Au solid state voltammetric microelectrodes were constructed from a 100 μm diameter Au wire immobilized in a Pyrex glass tube pulled to a tip of 0.4 mm diameter using marine epoxy and plated with mercury by electrodeposition of a $HgCl_2$ solution for 4 min at −0.1 V (Brendel and Luther, 1995). Voltammetric measurements were conducted in a three electrode configuration, including the Hg/Au voltammetric microelectrode, an Ag/AgCl reference electrode, and a Pt counter electrode using a computer-controlled DLK-70 potentiostat with DLK MAN-1 micromanipulator (Analytical Instrument Systems, Inc.). Dissolved O_2 was determined by linear sweep voltammetry (LSV) between −0.1 and − 1.75 V at a scan rate of 200 mV/s with an initial conditioning step of 10 s at −0.1 V and calibrated in situ using temperature and salinity of the overlying water assuming oxygen was at saturation (Luther et al., 2008). All other species were determined by cathodic square-wave voltammetry (CSWV), between −0.1 and − 1.75 V at a scan rate of 200 mV/s with a conditioning step of 10 s at −0.1 V (Brendel and Luther, 1995). When org-Fe(III) or ΣH_2S were detected, an additional conditioning step of 10 s at −0.9 V was included prior the above procedure to clean the electrode (Taillefert et al., 2000b). Electrodes were calibrated for Mn^{2+} by CSWV with $MnCl_2$, and Mn^{2+} sensitivities were used to quantify Fe^{2+} and ΣH_2S according to the pilot ion method (Luther et al., 2008). As org-Fe(III) and FeS_{aq} are not quantifiable, reported current intensities are normalized to average electrode sensitivity (Tercier-Waeber and Taillefert, 2008). All voltammetric data were integrated using VOLTINT, a semi-automated Matlab script with peak recognition software (Bristow and Taillefert, 2008). Depth profiles of pH were simultaneously obtained by deploying a 10 cm long MI-414B needle combination pH minielectrode (Microelectrodes, Inc.) calibrated with TRIS buffer in synthetic seawater (Dickson, 1993) within 5 mm laterally from the Hg/Au voltammetric microelectrode.

After voltammetric profiling, pore waters were extracted from the same sediment cores in a glove bag (Sigma-Aldrich) extensively flushed with N_2 gas to avoid air contaminations. The overlying water was sampled and the sediment sectioned in 6–10 mm sections under N_2 atmosphere. The sediment sections were then centrifuged at 3000 rpm for 10 min and filtered using 0.2 μm Puradisc polyethersulfone (PES) syringe filters (Whatman) both under N_2 atmosphere. For sandy sediments, a screen insert was added to the centrifuge tubes to allow separation of pore waters from the above sediment during centrifugation. Filtered pore waters were then partitioned under N_2 atmosphere for onboard analyses of total dissolved orthophosphate (ΣPO_4^{3-}) and dissolved inorganic carbon (DIC). Total dissolved orthophosphate (ΣPO_4^{3-}) was quantified spectrophotometrically using the paramolybdate method (Murphy and Riley, 1962), whereas DIC was analyzed by flow injection analysis (Hall and Aller, 1992) with a conductivity meter (Fisher Scientifics, Inc.) and a computer-controlled LCC-100 Integrator (AIS, Inc.). The remaining pore waters and solid sediments were frozen for analysis of inorganic anions (Cl^-, Br^-, NO_2^-, NO_3^-, SO_4^{2-}) in the dissolved phase and iron in the solid phase back at Georgia Tech. Inorganic anions (Cl^-, Br^-, NO_2^-, NO_3^-, SO_4^{2-}) were determined in one step by high pressure liquid chromatography (HPLC) using a Metrohm Metrosep A supp 5 anion exchange column (150 mm × 4 mm) with a 3.2 mM Na_2CO_3/1.0 mM $NaHCO_3$ eluent, flow rate of 0.7 mL/min, and UV detection at 215 nm (Beckler et al., 2014). Finally, highly reactive and total Fe(III) (oxyhydr)oxides (hereafter referred to simply as Fe(III) oxides) were extracted using ascorbate and dithionite reagents, respectively (Kostka and Luther, 1994), and quantified using the ferrozine method (Stookey, 1970). Crystalline Fe(III) oxides were quantified by difference between dithionite and ascorbate iron extractions, and both reactive and crystalline Fe(III) oxides were normalized to the mass of dry sediment, which was determined along with porosity in subsamples by weighing before and after drying at 40 °C for several days.

2.3. Calculations

Diffusive oxygen uptake (DOU) was calculated across the sediment-water interface and maximum diffusive fluxes of Fe^{2+}, HPO_4^{2-} (as proxy for ΣPO_4^{3-}), and HS^- (as proxy for ΣH_2S) were determined from the steepest portion of pore water gradients in concentration of each species. As the steepest pore water gradient may occur at any depth within the sediment, the maximum diffusive fluxes do not provide direct information about the benthic flux across the sediment water interface but instead provides a metric for compairing dominant biogeochemical processes between sediment cores. Both DOU and maximum diffusive fluxes were calculated following a modification of Fick's first law to account for tortuosity (θ) (Boudreau, 1997):

$$F_x = -\varphi \frac{D_x^0}{\theta^2} \frac{dC_x}{dz} \quad (1)$$

where F_x is the diffusive flux of species x, φ is the sediment porosity, D_x^0 is the ionic or molecular diffusion coefficient of species x, C_x is the concentration of species x, and z is sediment depth. The tortuosity was estimated from Archie's law ($\theta^2 = \varphi^{(1-m)}$) with m = 2 for φ ≤ 0.7 and m = 2.5 for φ = 0.7–0.9 (Ullman and Aller, 1982). The molecular diffusion coefficient for dissolved O_2, Fe^{2+}, HPO_4^{2-}, and HS^- were calculated based on temperature and the dynamic viscosity (μ) of seawater at the temperature, pressure, and salinity of the site:

$$D_{O_2}^0 = \left(m_0 + m_1 \frac{T}{\mu}\right) x10^{-5} \quad (2)$$

$$D^0_{(Fe^{2+}, HPO_4^{2-}, HS^-)} = (m_0 + m_1 \bullet T) x10^{-6} \quad (3)$$

where m_0 and m_1 are constants determined for each species (Boudreau, 1997). Molecular diffusion coefficient constants for HPO_4^{2-} and HS^- were determined to be sufficient for calculations of ΣPO_4^{3-} and ΣH_2S over the pH range measured. As the composition of the org-Fe(III) complexes is unknown, the molecular diffusion coefficient was estimated from the Stokes-Einstein equation (Cornel et al., 1986), assuming spherical org-Fe(III) species (Eq. (4)),

$$D^0_{Org-Fe(III)} = \frac{kT}{6\pi\mu\left(\frac{3}{4\pi}\frac{MW}{\rho N}\right)^{1/3}}\ cm^2 s^{-1} \quad (4)$$

where k is the Boltzmann constant, T is temperature, μ is the dynamic viscosity, ρ is density, N is Avogadro's number, and MW is the molecular weight. A model molecular weight of 1 kDa was chosen along with a density of 1.13 g cm^{-3} based on humic-like substances (Jones et al., 2011). Diffusive fluxes into the oxic zone (as determined by the detection of dissolved O_2) were calculated for individual species when appropriate. Bioturbation is omitted in flux calculations as the pore fluid exchange rates at these locations is not known.

Whole core depth-integrated pore water concentrations (Z) of each species (x) were calculated at each station by integrating the concentration of each species over the thickness of each core section then dividing by the total core depth length:

$$Z_x = \frac{\varphi \int_0^{z_f} C_x dz}{z_f} \quad (5)$$

where φ is the sediment porosity, C_x is the concentration of species x (moles/l), z is the thickness of each core section (mm), and z_f is the total core length (mm). By providing the stock of each redox species, whole core depth-integrated pore water concentrations provide an alternative method to compare dominant biogeochemical processes between sediment cores across the continental margin.

2.4. Sediment incubations

Sediment slurry incubations were carried out with sediments from four stations (6B, 6C, 7 and 11) collected in 2015. Bulk sections from within and outside org-Fe(III) production zones at stations 6B (0–8; 8–16; 30–38 cm), 6C (0–5; 5–12; 12–24; 24–35 cm), 7 (0–4; 4–10; 10–18; 18–24; 24–30 cm), and 11 (0–5; 5–11; 11–22; 22–33 cm) were homogenized and incubated. Homogenized sediment (~20% *v*/v) was mixed with the overlying water of each site in 28 mL hungate tubes (Chemglass), degassed for 10 min to remove the majority of dissolved oxygen, wrapped in tin foil, and placed on a rotary wheel (Fisher Scientific, Inc.). Samples were collected over time and filtered inside an anaerobic chamber (N_2 atmosphere) to prevent chemical oxidation of Fe^{2+}. Dissolved Fe^{2+} and total dissolved iron were measured spectrophotometrically by the Ferrozine method in each sample before and after addition of hydroxylamine, and dissolved Fe(III) was determined as the difference between total dissolved iron and Fe^{2+} concentrations (Stookey, 1970). Analysis of pore water SO_4^{2-} was conducted by HPLC using the same procedures described above. Production rates of dissolved iron were calculated from the slope of the linear regression of concentration versus time at different depth intervals. For comparison to diffusive fluxes, depth-integrated rates (mmol cm^{-2} day^{-1}) were determined in the top incubation section at each station (Eq. 6):

$$\text{Depth} - \text{integrated rate}_x = \varphi \int_{z_i}^{z_f} R_x(z) dz \quad (6)$$

where φ is the sediment porosity, $R_x(z)$ is the depth distribution of the production of species x (mmol cm^{-3} day^{-1}), z_i is initial depth of the incubation zone (cm), and z_f is the final depth of the incubation zone (Canfield, 1989).

3. Results

3.1. Bottom water characteristics

Water depth determined along the transect between 34.6802 N 76.6469 W and 33.4706 N 75.5169 W (Fig. 1 black line) are represented against distance from shore (Fig. 2). Past the coastal zone (0–20 m), the continental shelf (20–50 m) had an average gradient of 0.03 ± 0.5° (Fig. 2). The continental slope spans the outer margin of the continental shelf, beginning at the shelf break at ~50 m and extending to a depth of 2600 m. It can be divided into three subcategories: the upper-slope (50–500 m), mid-slope (500–900 m), and lower slope (900–2600 m) with average gradients of 0.73 ± 0.4°, 1.9 ± 0.7°, and 5.6 ± 1.4° (Fig. 2). Below 2600 m, the gradient decreases to 0.73 ± 0.6°, indicating the beginning of the continental rise. Bottom water temperatures decreased proportionally to water column depth (Table 1, Fig. 2). At all stations bottom water salinities averaged 36 ± 2 (Table 1). The water column was fully oxygenated across the entire transect with bottom water concentrations averaging 0.223 ± 0.02 mM (Table 1).

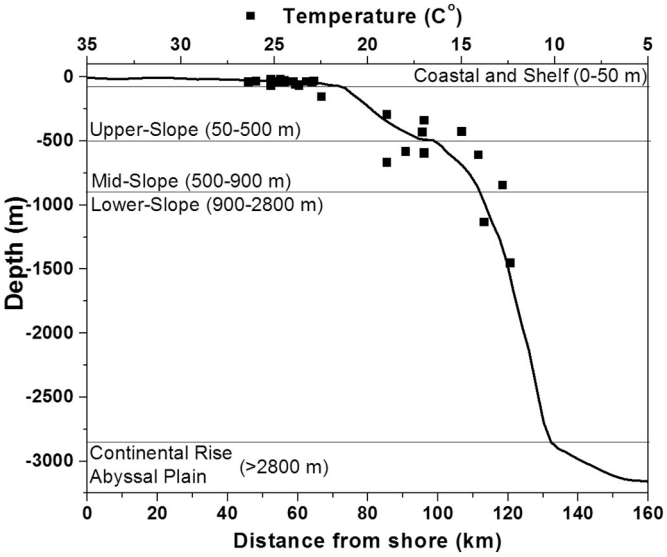

Fig. 2. Bottom water temperature (°C) as a function of water depth (scatter points) and water depth as a function of distance from shore (black line) along the transect shown in Fig. 1.

3.2. Pore water depth profiles

Oxygen penetration depths (OPD) were small at coastal stations with an average of 2.5 ± 0.7 mm at all stations sampled nearshore (e.g., St. CL), increased from an average of 5 ± 6 to 15 ± 6 mm from the shelf (e.g., St. 2) to the upper-slope (e.g., St. 8, 6B, 7), then decreased to an average of 10 ± 2 mm on the mid-slope (e.g., St. 5, 11, 13). Finally, the OPD increased on the lower slope to an average of 20 ± 6 mm (e.g., St. 13B and 14) (Figs. 3 and S1-S4). Except for the mid-slope stations (Fig. S4), neither dissolved Fe^{2+} or org-Fe(III) was detected in the oxic zone of any sediment core along the transect. At the coastal station (St. CL), dissolved Fe^{2+} concentrations remained below detection limit (< 20 μM) (Fig. S1) or oscillated up to 170 μM above the onset of sulfide production and increased as current intensities of org-Fe (III) complexes simultaneously decreased (Fig. 3). In turn, ΣH_2S and FeS_{aq} were below detection limit in the zone of iron reduction but increased with depth up to 230 μM and 20 nA, respectively, once Fe^{2+} and org-Fe(III) complexes were depleted (Fig. 3). Sulfate reduction was evidenced each year this station was investigated by the overall production of 140–230 μM ΣH_2S at variable depths in the sediment column (Fig. S1). Additionally, St. CL was the only location on the continental margin where Mn^{2+} was observed with peaks up to 70 μM at 32 mm depth in 2015 (Fig. 3) and similar concentrations and location in the depth profile measured in 2012 (Fig. S1). On the continental shelf (St. 1,2,3, and 4), Fe^{2+} and org-Fe(III) were not observed in the pore waters (e.g., St. 2 in Fig. 3) except at stations 4 (Fig. S2), where the onset of Fe^{2+} occurred at 46 ± 7 mm on average between 2015 and 2016 with maximum concentrations of 99 μM, while org-Fe(III) onset was slightly shallower at 38 ± 4 mm and had maximum signals of 8 nA. Although

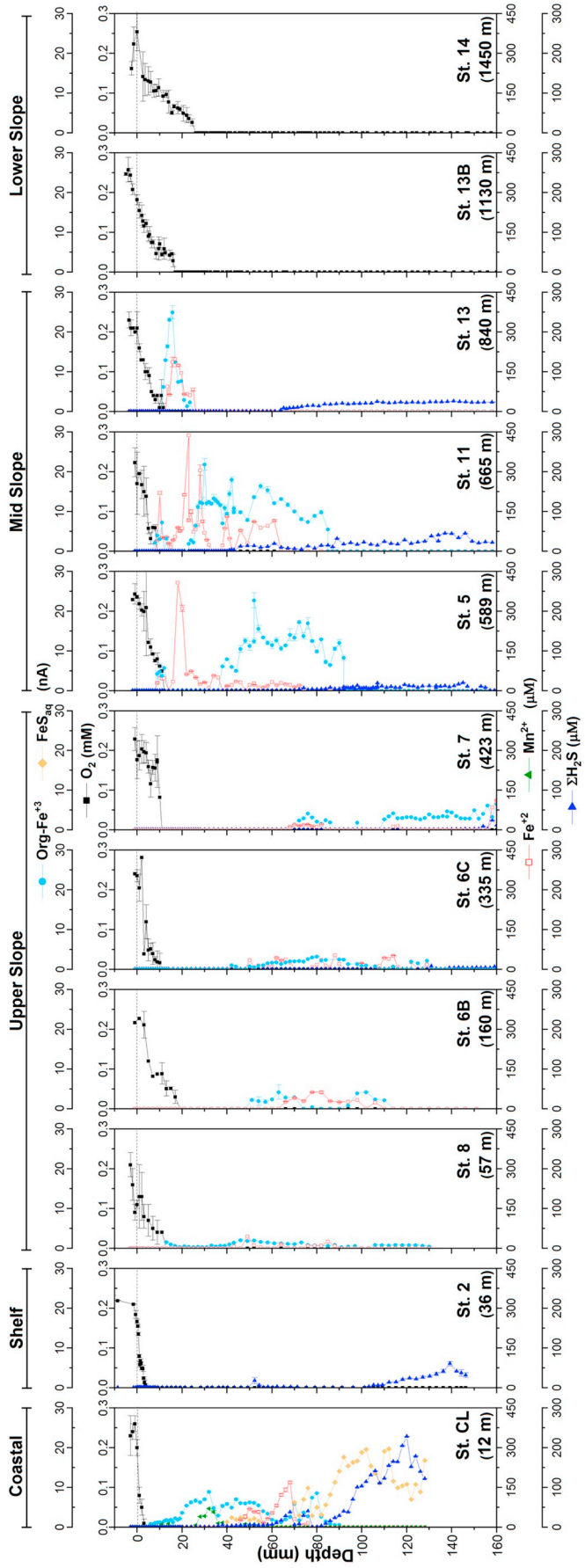

Fig. 3. Depth profiles of dissolved O_2, Fe^{2+}, organic-Fe(III), FeS_{aq}, Mn^{2+}, and ΣH_2S concentrations measured electrochemically in representative sediment cores as a function of water column depth between 2012 and 2016: coastal (St. CL), shelf (St. 2), upper-slope (St. 8, 6B, 7), mid-slope (St. 5, 11, 13), lower-slope (St. 13B, 14).

ΣH_2S was detected sporadically at every station on the shelf (e.g., St. 2 in Fig. 3), a wide ΣH_2S onset depth of 77 ± 31 mm was observed between 2010 and 2016 (Figs. S1–S2). Similar to St. 4, Fe^{2+} and org-Fe (III) generally formed broad peaks at 52 ± 18 and 51 ± 11 mm on average between upper-slope stations (St. 6, 6B, 6C, 7, 7B, 8, and 9), and their concentrations and current intensities reached maximum concentrations ranging between 40 and 110 μM and between 2 and 10 nA (Figs. 3 and S3). In turn, the onset of ΣH_2S descended to 108 ± 35 mm on average between 2015 and 2016 at these stations, when detected (Figs. 3 and S3). On the mid-slope (St. 5, 10, 11, 12, and 13), the onset of dissolved Fe^{2+} and org-Fe(III) rose to 12 ± 5 and 22 ± 12 mm on average, close to the OPD, while ΣH_2S production also rose to 73 ± 32 mm with concentrations reaching maximums of 437 μM Fe^{2+} at St. 11 and 24 nA org-Fe(III) at St. 13 (Figs. 3 and S4). Finally, pore water Fe^{2+}, org-Fe(III), and ΣH_2S were not detected at any depth in the profiles on the lower slope (St. 13B and 14 in Fig. 3).

DIC concentrations either increased slightly (<5 mM) or remained relatively constant with depth at all locations (Figs. 4 and S5–S8). No significant changes in SO_4^{2-} were observed in any of the stations (Figs. 4 and S5–S8), except for a subsurface minimum in the first few centimeters at the deepest station (St. 14). In turn, ΣPO_4^{3-} produced subsurface maxima up to 15 μM at 30 mm in the coastal zone (St. CL), but did not reach concentrations above 7 μM on most of the shelf or shallow upper-slope stations (St. 1, 2, 3, 4, 6B, 8, and 9 in Fig. 4 and Figs. S5–S7). Although ΣPO_4^{3-} concentrations maxima remained low at St. 7, with just 8 μM observed at 103 mm, ΣPO_4^{3-} concentrations generally increased as water depth increased (St. 6, 6C, and 7B in Figs. 4 and S7). At St. 6C a maximum concentration of 22 μM was observed at 63 mm. On the mid-slope, ΣPO_4^{3-} increased to maximum concentrations of 16 ± 3 μM at 54 ± 5 mm on average between stations (St. 5, 10, and 11 in Figs. 4 and S8). Deeper on the mid-slope (St. 13) and into the lower-slope (St. 13B), ΣPO_4^{3-} maxima reached shallower depths (44 ± 2 mm) but in lower concentrations (12 ± 3 μM) on average between these stations (Fig. 4). Finally, ΣPO_4^{3-} gradually increased to 10 μM at 173 mm at the deepest location (St. 14).

3.3. Solid phase iron depth profiles

Almost no reactive Fe(III) oxides, as determined by ascorbate extraction, were detected in the shallow upper-slope sediments (St. 8 and 6B in Fig. 5). Reactive Fe(III) oxide concentrations, however, generally formed subsurface maxima near the sediment-water interface that increased with water column depth to concentrations up to 6 and 5.8 μmol Fe/g dry weight (gdw) in the top 20 mm on the upper-slope (St. 6C and St. 7 in Fig. 5) and up to 8.8 μmol Fe/gdw in the top 20 mm on the mid-slope (St. 5). Concentrations in the top 20 mm decreased with water depth from the mid to lower-slope (7.2 μmol Fe/gdw was observed at St. 11, 4.5 μmol Fe/gdw at St. 13, and 4.3 μmol Fe/gdw at St. 13B). Interestingly, concentrations of reactive Fe(III) oxides were as high as 7.2 μmol Fe/gdw in the top 30 mm at the deepest station (St. 14). At all stations except for the upper and mid-slopes (St. 6C, 7, 5, and 11), the concentration of reactive Fe(III) oxides was <1.5 μmol Fe/gdw below 40 mm.

Crystalline Fe(III) oxides, as determined by the difference between dithionite extractable and ascorbate extractable iron, only reached concentrations up to 13.7 and 15.4 μmol Fe/gdw on the shallow upper-slope (St. 8 and 6B) and remained constant with sediment depth (Fig. 5). In turn, concentrations gradually decreased from 17.9 and 27.4 μmol Fe/gdw in the top 20 mm to 8.2 and 8.1 μmol Fe/gdw by 180

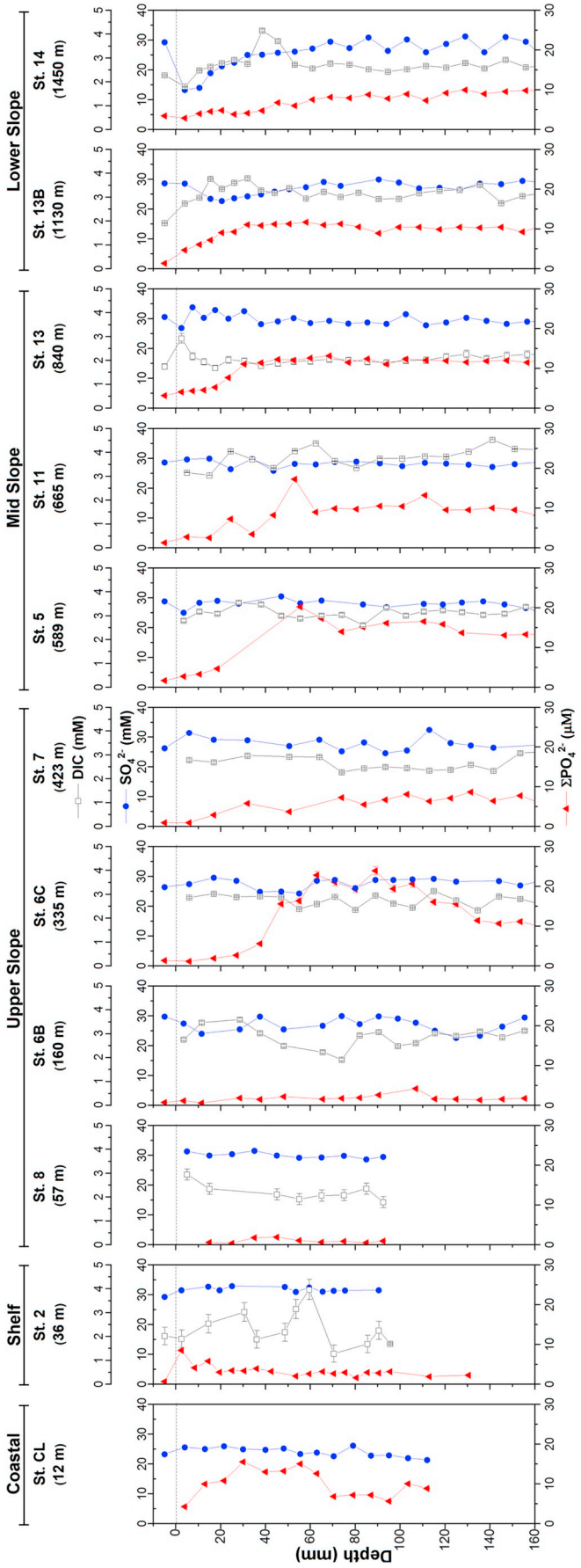

Fig. 4. Depth profiles of dissolved DIC, SO_4^{2-} and ΣPO_4^{3-} concentrations measured in pore waters of representative sediment cores as a function of water column depth between 2012 and 2016: coastal (St. CL), shelf (St. 2), upper slope (St. 8, 6B, 7), mid-slope (St. 5, 11, 13), lower-slope (St. 13B, 14).

and 237 mm at St. 6C and St. 7, though a small rebound to 18.2 μmol Fe/gdw was observed at 74 mm in the St. 7 sediment core. Crystalline Fe(III) oxide concentrations were the highest on the mid-slope, with concentrations up to 50.9 and 38.2 μmol Fe/gdw in the top 20 mm of St. 5 and St. 11 (Fig. 5). However, concentrations decreased sharply to 20 μmol Fe/gdw at 28 mm, then gradually decreased to 10.1 μmol Fe/gdw at 207 mm at St. 5, whereas the concentrations gradually decreased to 18.47 μmol Fe/gdw at 213 mm at St. 11. Crystalline Fe(III) oxide concentrations decreased with increased water depth on the mid-slope (Fig. 5). At St. 13 crystalline Fe(III) oxides reached concentrations of 20.4 μmol Fe/gdw in the top 20 cm, decreased to 7.8 μmol Fe/gdw between 20 and 53 mm, rebounded to 14.5 μmol Fe/gdw, and were followed by a gradual decrease with depth below 70 mm. Similar patterns were observed at St. 13B, albeit at concentrations peaking at 33.3 μmol Fe/gdw around 20 mm, decreasing to 6.6 μmol Fe/gdw at 50 mm, rebounding to 20.4 μmol Fe/gdw at 66 mm, and then decreasing with depth below 110 mm. Although concentrations as high as 3.9 μmol Fe/gdw were determined in the top 35 mm at St.14, crystalline Fe(III) oxide concentrations were generally low and decreased with depth to 1.1 μmol Fe/gdw.

3.4. Sediment incubations

Concentrations of both dissolved Fe^{2+} and dissolved Fe(III) generally increased over the 52-day incubation period whereas no change in SO_4^{2-} concentrations was observed in any of the incubations (Fig. S9). Minimal dissolved Fe^{2+} and Fe(III) were produced during incubations of any sediment sections from the shallow (St. 6B; 150 m water depth) and middle (St. 6C; 335 m water depth) upper-slope sediments (Fig. S9), and similar Fe^{2+} production rates were observed at both stations (Fig. 6A), reflecting the generally low Fe^{2+} concentrations and org-Fe(III) current intensities measured in the depth profiles (Fig. 3). Simultaneously, higher concentrations (Fig. S9) and higher production rates (Fig. 6B) of dissolved Fe(III) were observed at St. 6C than St. 6B, and rates tended to decrease with depth below the sediment-water interface at St. 6C while they remained constant with depth at St. 6B. Deeper on the upper-slope (St.7; 423 m water depth), Fe^{2+} production rates were generally higher and increased slightly with sediment depth below 7 cm (Fig. 6A), while dissolved Fe(III) production rates were maximum at 7 cm and generally decreased deeper in the sediment (Fig. 6B). Both Fe^{2+} and org-Fe(III) complexes formed small peaks between 4 and 10 cm with depth in the pore waters (Fig. 3), whereas small concentrations of Fe^{2+} and ΣH_2S and a broad but small org-Fe(III) signal was detected between 10 and 24 cm in St. 7 sediments. The highest rates of both Fe^{2+} and Fe(III) production were observed on the mid-shelf (St. 11; 665 m water depth), where rates of 4.6 ± 0.4 μM Fe^{2+} day^{-1} (Fig. 6A) and 7.7 ± 0.3 μM Fe(III) day^{-1} (Fig. 6B) were measured in the first 5 cm of the sediment, but decreased to stabilize around 1.8 ± 0.1 μM Fe^{2+} day^{-1} and 2.2 ± 0.3 μM Fe(III) day^{-1} below 16 cm. The high rates in Fe^{2+} and dissolved Fe(III) production coincided with the high Fe^{2+} concentrations and org-Fe(III) current intensities detected in the top 5 cm of the sediment and their disappearance below the onset depth of dissolved sulfide at 4.5 cm (Fig. 3).

3.5. DOU, maximum diffusive fluxes, and whole core concentrations

DOU was highest in the coastal zone with an average of 2.9 ± 0.8 $mmol/m^2/day$, decreased from the shelf (0.9 ± 0.2 $mmol/m^2/day$) to the upper-slope (0.6 ± 0.3 $mmol/m^2/day$), rebounded on

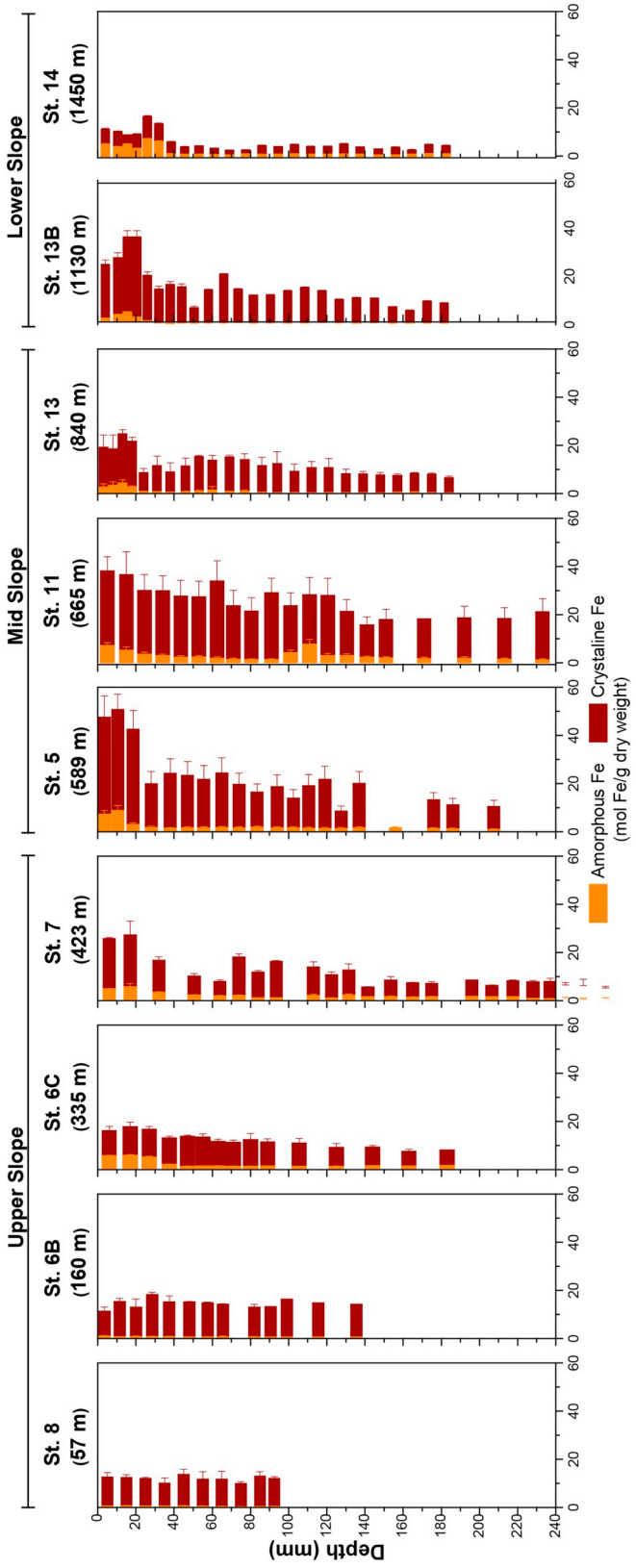

Fig. 5. Depth profiles of amorphous Fe(III)-oxides determined by ascorbate extraction and total iron oxides (amorphous and crystalline Fe(III)-oxides, AVS) determined by dithionite extraction in representative sediments from the upper slope to the lower slope between 2015 and 2016.

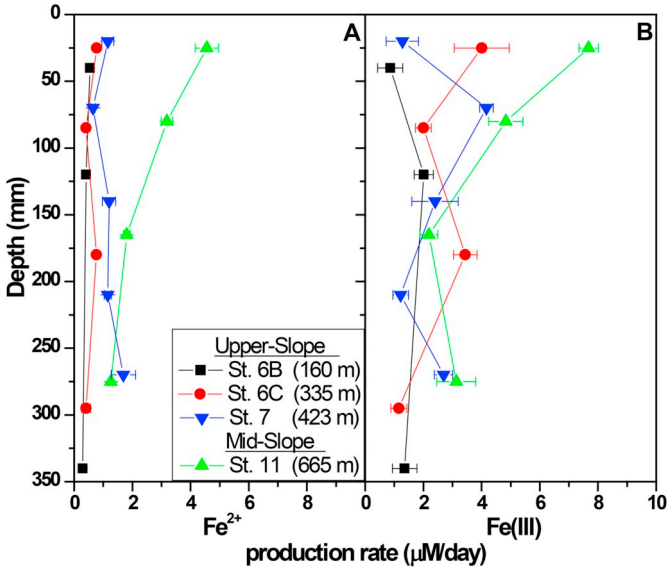

Fig. 6. Depth distributions of (A) dissolved Fe^{2+} and (B) Fe(III) production rates determined from sediment slurry incubations. Error bars represent the standard deviation of the slope of regression lines of concentration vs. time for duplicate incubations.

the mid-slope (1.9 ± 0.7 mmol/m^2/day), and ultimately decreased on the lower-slope (0.8 ± 0.2 mmol/m^2/day) (averages and ranges in Table S1, Fig. 7A). Similarly, maximum diffusive fluxes of Fe^{2+}, org-Fe (III), and ΣPO_4^{3-} were high in the coastal zone, decreased in the shelf and upper-slope, reached maximum values in the mid-slope, then decreased again in the lower-slope (Table S1, Fig. 7B,C). While maximum diffusive ΣH_2S fluxes were low in the upper-slope, values calculated in the coastal zone and the shelf were larger than the maximum diffusive fluxes calculated in mid-slope sediments (Table S1, Fig. 7B). Despite production of dissolved Fe^{2+} and org-Fe(III) into the oxic zone, diffusive fluxes across the sediment-water interface were not detected at any station along the continental margin.

Whole core depth-integrated pore water concentrations calculated for Fe^{2+} reached values up to 7.3 μM in the coastal zone and decreased to below 3.0 μM in the shelf. In the upper-slope, whole core Fe^{2+} concentrations were below 5.2 μM, increased to values between 4.9 and 40.5 μM in the mid-slope, and were below detection in the lower-slope (Table S2, Fig. 8). Whole core depth-integrated concentrations of org-Fe (III) were similar in the coastal, shelf, and upper-slope, not reaching values >1.3 nA, however in the mid-slope values up to 6.1 nA was calculated. Similar to Fe^{2+}, org-Fe(III) was below detection in the lower-slope. Whole core depth-integrated concentrations of ΣH_2S were the highest in the coastal zone, reaching concentrations up to 25.9 μM. However, ΣH_2S concentrations generally decreased from the shelf (<13.2 μM) to the upper-slope (<0.8 μM), rebounded on the mid-slope (<12.7 μM), albeit to concentrations lower than the shelf, and were below detection on the lower-slope.

4. Discussion

Although the benthic production of iron from continental shelves (Elrod et al., 2004; Noffke et al., 2012; Severmann et al., 2010) and its effect on the supply of iron to the water column (Bruland et al., 2001; Fitzwater et al., 2003; Johnson et al., 1999; Lohan and Bruland, 2008) have been demonstrated and used to extrapolate global sedimentary iron fluxes from continental margins (Dale et al., 2015), these estimates may be biased by the number of studies investigating the iron flux in upwelling zones that are not representative of the majority of the oceans. In this study, the production of dissolved iron and the biogeochemical processes responsible for its production were examined in

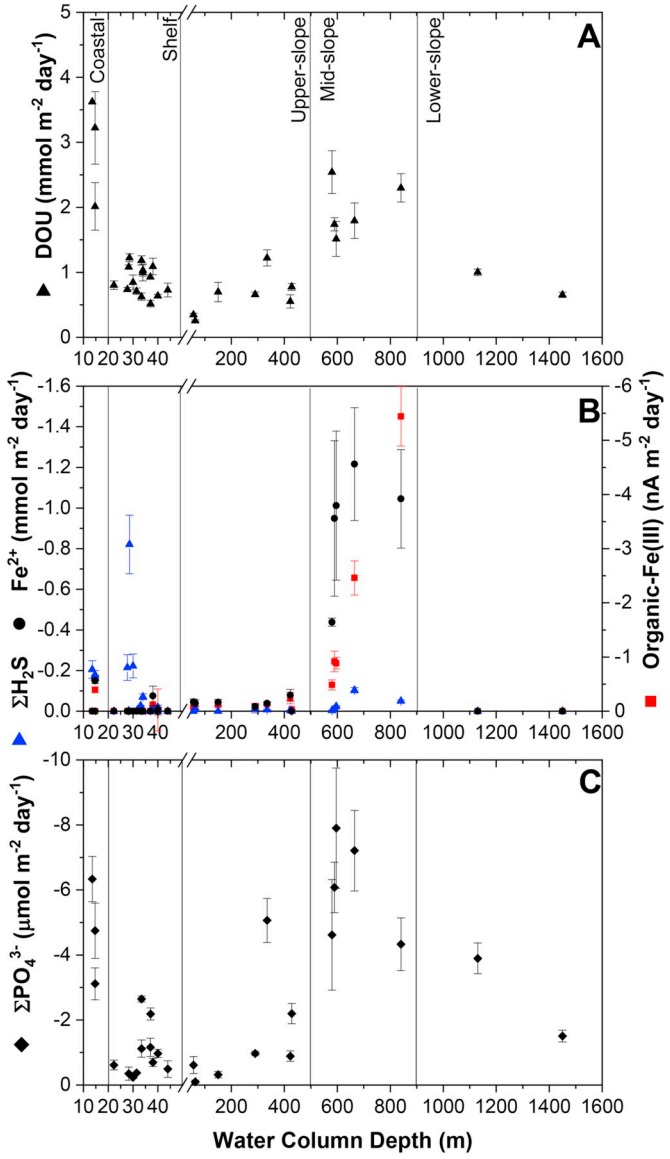

Fig. 7. (A) Diffusive oxygen uptake (DOU), (B) Maximum diffusive fluxes of dissolved Fe^{2+}, org-Fe(III) complexes, and ΣH_2S, and (C) Maximum diffusive flux of ΣPO_4^{3-} with water column depth across the continental margin sediments of Cape Lookout (NC). Maximum diffusive fluxes were calculated at the depth of the steepest portion of the pore water gradients to compare the intensity of biogeochemical processes in the different sediments across the continental margin. Diffusive fluxes of Fe^{2+} and org-Fe(III) across the sediment-water interface remained below detection limit.

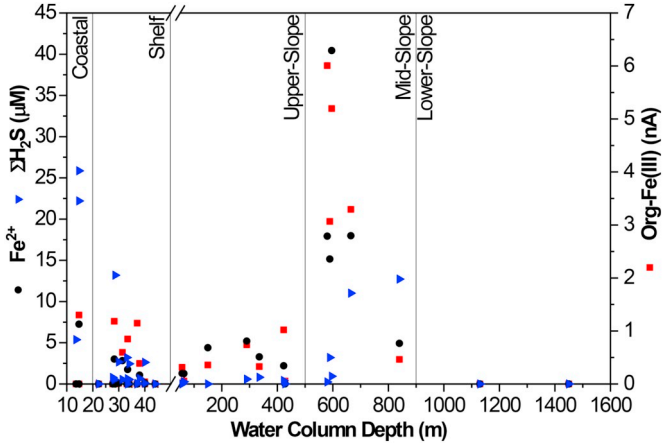

Fig. 8. Whole core concentrations of dissolved Fe^{2+}, organic-Fe^{3+}, and ΣH_2S with water column depth across the continental margin of Cape Lookout between 2010 and 2016. Whole core concentrations were obtained by integrating the mole content of each species as a function of depth and normalizing to the total volume of each sediment core.

continental margin sediments with limited upwelling and sediment resuspension (Csanady and Hamilton, 1988; Janowitz and Pietrafesa, 1980; Pietrafesa et al., 1985).

4.1. Continental slopes as zones of enhanced carbon remineralization processes

The variations in maximum diffusive fluxes (Fig. 7) and depth-integrated concentrations (Fig. 8) of all pore water species as a function of water column depth across Cape Lookout's continental margin reflect the changes in carbon remineralization processes across a passive continental margin not exposed to significant riverine inputs or upwelling. DOU (Fig. 7A), maximum diffusive fluxes of Fe^{2+}, org-Fe(III) complexes, and ΣPO_4^{3-} (Fig. 7B and C), and depth-integrated concentrations (Fig. 8) all decreased from the coast, exposed to significant inputs of organic matter, to the shelf and upper-slope, as the inputs of organic matter subsided offshore, then rebounded on the mid-slope, and decreased again on the lower-slope. Reactive and crystalline Fe(III) oxide concentrations also increased in the top 20 cm of mid-slope sediments relative to continental shelf and lower-slope sediments (Fig. 5). Sediment slurry incubations demonstrated similar changes with water depth (Fig. 6), as rates of both Fe^{2+} and Fe(III) production gradually increased from the shallow upper slope (St. 6B, 6C, and 7) to the mid-slope (St. 11). These results provide evidence that the mid-slope off Cape Lookout can be considered a depocenter where the influx of organic matter and terrigenous material increases aerobic and anaerobic respiration processes in these sediments compared to the continental shelf. The formation of such depocenters is supported by the low physical turbulence typically observed in upper slope sediments (Csanady, 1990) and the high flux and accumulation of sediment on the mid-slope of the Mid-Atlantic Bight (Biscaye et al., 1988) and Carolina coast (DeMaster et al., 1994; Diaz et al., 1994). Incubations have demonstrated that microbial populations are not nutrient limited in mid-slope relative to continental shelf sediments across the Mid-Atlantic Bight (Kemp, 1994). Additionally, given the high concentrations of organic carbon observed in a number of continental slope sediments relative to the shelf, including Cape Hatteras as well as to the north and south of the Carolina coast (Alperin et al., 2002; Blake et al., 1987; DeMaster et al., 1994; Milliman, 1994; Schaff et al., 1992), across the mid-Atlantic Bight (Anderson et al., 1994; Walsh et al., 1988; Walsh et al., 1985), Bering Sea (Walsh et al., 1985), Peru coast (Noffke et al., 2012; Walsh et al., 1985), the Oman margin of the Arabian Sea (Pedersen et al., 1992), the Washington coast (Carpenter, 1987), the Santa Catalina Basin (Smith et al., 1987), and near Monterey Bay (Murray and Kuivila, 1990), it seems that all slopes may represent organic carbon depocenters (Premuzic et al., 1982; Walsh et al., 1985). Thus, slope sediments from continental margins exposed or not to intense upwelling appear to be zones of increased microbial activity, which may potentially influence global ocean cycles.

4.2. Processes responsible for benthic oxygen consumption

Dissolved oxygen consumption in marine sediments results either from aerobic respiration or re-oxidation of the reduced inorganic products of anaerobic respiration (i.e., Mn^{2+}, Fe^{2+}, ΣH_2S, and NH_4^+) via abiotic or microbial processes. Although the relative importance of these two processes towards DOU cannot be directly quantified, knowledge of the environment and the biogeochemical processes

occurring deeper in the sediment may provide insight into the main mechanism of oxygen consumption. DOU measured in this study is likely underestimated compared to in situ oxygen uptake rates as a result of the strong effect of physical forcing (tidal pumping or bottom currents) on benthic exchange processes that are suppressed with sediment collection. Bioturbation, which may enhance sediment irrigation (Aller, 1982) and particle subduction (Levin et al., 1997), is also not easily captured by microelectrode depth profiles. However, even in the relatively more active Cape Hatteras transects to the north of Cape Lookout, little evidence for consistent attenuation of bioturbation intensity with water column depth has been reported (Alperin et al., 1999; Green et al., 2002; Diaz et al., 1994). In fact, macrofauna has been observed in similarly sediment densities as a function of water column depth along continental margin transects of both Cape Hatteras and Cape Lookout (Blake et al., 1987; Blake and Grassle, 1994; Blake and Hilbig, 1994; Aller et al., 2002). These studies suggest that bioturbation intensity does not vary significantly across the continental slope. Although comparison in bioturbation between shelf (< 50 m) and slope stations off the coast of North Carolina are lacking, bioturbation rates are generally higher in shelf compared to slope sediments (Archer and Devol, 1992; Esch et al., 2013). As all sediments were examined under diffusion controlled conditions and the effect of bioturbation was not captured by depth profiles with microelectrodes, the relative variation in DOU measured in sediment cores across the continental margin mainly reflects variations in biogeochemical conditions between locations.

The relatively high DOU measured in the coastal zone (Fig. 7A) can be attributed to the relatively high input of organic matter and terrigenous material to the sediment. In these sediments, dissolved O_2 was likely consumed via both aerobic respiration and re-oxidation of the reduced compounds produced by anaerobic respiration at depth. Indeed, relatively large concentrations of anaerobic respiration products were observed at St. CL (Fig. 3), including ΣH_2S and $FeS_{(aq)}$, which may be produced during the reduction of Fe(III) by ΣH_2S. These findings indicate that microbial sulfate reduction (MSR) was ongoing in these sediments despite no significant changes in SO_4^{2-} profiles (Fig. 4). Although the gap between the OPD and the onset depth of Fe^{2+} (43 mm) and ΣH_2S (74 ± 48 mm) was quiet significant at these stations, the close presence of Mn^{2+} to the oxic zone (i.e., 11 ± 8 mm) (Figs. 3 and S1) suggests reoxidation of reduced metabolites by dissolved oxygen. Similarly, the relatively higher intensity of carbon remineralization processes in these sediments may have contributed to significant nitrification near the sediment-water interface and thus consumption of dissolved oxygen. Over the shelf, DOU generally decreased with water column depth as continental inputs dissipated, following previous observations of the decrease in sediment oxygen demand with water depth (Heip et al., 1995; Kemp et al., 1992). As shelf sediment became dominated by sand and the iron content of these sediments is low (Fig. 5), decreased concentrations of dissolved anaerobic respiration products were detected (Figs. 3 and S1–S2) and the majority of O_2 consumption was likely due to aerobic respiration. Indeed, Mn^{2+} was not detected in any shelf sediments, and Fe^{2+} and ΣH_2S were either not detected or occurred well below the OPD. Whole core incubations of similar shelf sediments under diffusive conditions showed little build up of dissolved manganese and iron over time despite high inputs of organic matter fueled by benthic primary production (Jahnke et al., 2005). The low MSR activity revealed by the low ΣH_2S concentrations (Figs. 3, S3, and S8), the comparable concentrations of crystalline iron, and the low reactive Fe(III) oxides (Fig. 5) likely contributed to the similar and relatively stable DOU over the upper-slope (Fig. 7A). In addition, increased onset depths of dissolved Fe^{2+} with distance from shore along the upper-slope (Fig. 3) suggest that O_2 consumption was entirely controlled by aerobic respiration. As the sediment shifted from sand to silt and clay on the mid-slope and both reactive and crystalline Fe(III) oxide concentrations increased (Fig. 5), DOU increased simultaneously (Fig. 7A). Although the increased input of inorganic particulate material to the sediment is often accompanied by an increase in organic matter input which promotes aerobic respiration, detection of Fe^{2+} (Fig. 3) directly below the OPD points towards O_2 consumption linked to the reoxidation of reduced metabolites. Similar increases in oxygen demand observed in mid-slope sediments along the Mid-Atlantic Bight were attributed to lateral inputs of organic matter from the much larger continental shelf (Anderson et al., 1994; Rowe et al., 1994), and discrepancies between O_2 consumption maxima and patterns of aerobic bacterial production were attributed to subsequent reoxidation of reduced metabolites produced by anaerobic processes deeper in the sediment (Kemp, 1994). Finally, DOU decreased (Fig. 7A) concomitantly with the reactive and crystalline Fe(III) oxide concentrations (Fig. 5) on the lower-slope, as expected based on numerous observations of decreased sediment oxygen demand on the continental rise and abyssal plain (Glud, 2008).

4.3. Biogeochemical controls on sediment iron production

Although dissolved Fe^{2+} has been detected in sediment pore waters at water depths between 60 and 2000 m in zones of the Mid-Atlantic Bight, where upwelling is minimal and sulfate reduction does not contribute significantly to organic carbon remineralization, iron concentrations were not reported (Anderson et al., 1994). Similarly, production of dissolved iron has not been investigated on the Carolina coast (Alperin et al., 1999; Jahnke and Jahnke, 2000; Thomas et al., 2002). The millimeter resolution of pore water profiles collected in Cape Lookout continental margin sediments, backed up by maximum diffusive flux calculations and depth-integrated concentrations of pore water constituents demonstrate that dissolved iron is produced in these sediments and provides insight into the biogeochemical processes that regulate iron reduction and the potential release of iron across the sediment-water interface.

In the coastal zone, the maximum diffusive ΣH_2S flux was greater than the Fe^{2+} flux (Fig. 7B), though pore water profiles demonstrate that both Fe^{2+} and org-Fe(III) complexes were produced in the top 6 cm of these sediments (Fig. 3). As org-Fe(III) complexes are rapidly reduced by dissolved sulfide (Taillefert et al., 2000a), their presence is indicative of a lack of or insignificant sulfate reduction. Org-Fe(III) complexes may be formed either by abiotic oxidation of Fe^{2+} by dissolved O_2 (Taillefert et al., 2000a), aerobic Fe-oxidizing bacteria in the presence of organic ligands (Roden et al., 2004; Sobolev and Roden, 2001), abiotic oxidation of complexed Fe(II) by Fe(III) (Beckler et al., 2015; Luther et al., 1992), or non-reductive dissolution of Fe(III) oxides during dissimilatory iron reduction (DIR) (Beckler et al., 2015; Fennessey et al., 2010; Jones et al., 2010; Nevin and Lovley, 2002; Taillefert et al., 2007). Production of soluble org-Fe(III) complexes at much deeper depths than the OPD indicates that these species did likely not form via aerobic processes. However, it is difficult to determine if they were produced microbially or via chemical oxidation of complexed Fe(II). Detection of FeS_{aq} and ΣH_2S below Fe^{2+} in coastal zone sediments (St. CL, Fig. 3) points towards abiotic reduction of Fe(III) oxides by ΣH_2S (Beckler et al., 2016) and active precipitation of $FeS_{(s)}$ (Taillefert et al., 2000a). Simultaneouly, the production of soluble org-Fe(III) complexes at shallower depths than Fe^{2+} (St. CL, Fig. 3) suggests upward diffusion and abiotic oxidation of complexed Fe(II).

Similar maximum diffusive ΣH_2S fluxes (Fig. 7B) and depth-integrated ΣH_2S concentrations (Fig. 8) were observed on the shallow shelf and in the coastal zone, however, both decreased towards the upper-slope where only small ΣH_2S concentrations were detected. As Fe^{2+} or org-Fe(III) complexes were not detected in the shallow shelf pore waters besides St. 4 (Figs. 3 and S1–S2), MSR appears to be the main anaerobic respiration process on the continental shelf. Based on DOU (Fig. 7A), anaerobic respiration was expected to be lower in upper-slope compared to shelf sediments. Indeed, the generally low production rates of dissolved Fe^{2+} and Fe(III) in the slurry incubations with sediments from St. 6B, 6C, and 7 (Fig. 6) indicate reduced

Table 2
Maximum diffusive fluxes and depth-integrated rates of Fe^{2+} and dissolved Fe(III) production in the top section of incubated sediment from stations on the upper and mid-slope.

Station	Depth (m)	Fe^{2+}		Fe(III)	
		Maximum diffusive flux (mmol m^{-2} day^{-1})	Depth-integrated rate (mmol m^{-2} day^{-1})	Maximum diffusive flux (nA m^{-2} day^{-1})	Depth-integrated rate (mmol m^{-2} day^{-1})
6B	150	−0.044 ± 0.01	0.017 ± 0.0003	−0.119 ± 0.04	0.028 ± 0.0009
6C	335	−0.039 ± 0.01	0.017 ± 0.0002	−0.129 ± 0.02	0.090 ± 0.004
7	423	−0.078 ± 0.03	0.021 ± 0.0002	−0.244 ± 0.1	0.023 ± 0.0005
11	665	−1.22 ± 0.3	0.160 ± 0.005	−2.46 ± 0.3	0.269 ± 0.004

microbial activity in these sandy sediments. Maximum diffusive fluxes (Fig. 7B) and depth-integrated concentrations (Fig. 8) of Fe^{2+} and org-Fe(III) in both upper-slope and shelf sediments remained relatively low. Despite their low concentrations, both Fe^{2+} and org-Fe(III) complexes were detected at similar depths in the sediment of these three stations (Fig. 3, St. 6B, 6C, 7), suggesting that org-Fe(III) complexes were formed during DIR rather than as a result of Fe^{2+} oxidation. Increased concentrations (Fig. 4) and diffusive flux (Fig. 7C) of ΣPO_4^{3-} with water depth over the upper-slope point towards increased reduction of Fe(III) oxides (Anschutz et al., 1998; Rozan et al., 2002). In addition, no significant changes in SO_4^{2-} or DIC concentrations with depth (Fig. 4) and low or lack of ΣH_2S and FeS_{aq} (Fig. 3) suggest that MSR was limited in these sediments (Beckler et al., 2016). To identify the biogeochemical processes involved in the transformation and upward flux of iron in these sediments using independent techniques, depth-integrated rates of Fe^{2+} and dissolved Fe(III) production were calculated from the sediment incubations closest to the sediment-water interface and evaluated against the maximum diffusive fluxes at the same stations (Table 2). Both the depth-integrated rates of Fe^{2+} and dissolved Fe(III) from the sediment incubations and the maximum diffusive fluxes of Fe^{2+} and org-Fe(III) calculated from the depth profiles (Fig. 7B) generally increased with water column depth (Table 2), indicating that the underlying mechanism generating Fe^{2+} and dissolved Fe(III) are the same. Depth-integrated rates of dissolved Fe(III) cannot be directly compared to diffusive org-Fe(III) fluxes calculated from the depth profiles as org-Fe(III) cannot be quantified directly by voltammetry. Depth-integrated rates and diffusive fluxes of Fe^{2+} were roughly similar at the three upper-slope stations (St. 6B, 6C, and 7 in Table 2). However, these incubations did not perfectly mimic sediments at each site as they were conducted anaerobically and the sediment layers incubated did not always overlap with the zones where maximum diffusive fluxes were measured. As a result of the lack of O_2 and, therefore, limited reoxidation of Fe^{2+} during the incubations, depth-integrated rates of dissolved Fe(III) from the incubations may represent lower limits of Fe (III) production. Nonetheless, the sustained production of dissolved Fe (III) in the sediment incubations (Fig. S9) suggests that complexation by organic ligands stabilizes iron in solution in these sediments.

Although diffusive fluxes of Fe^{2+} and org-Fe(III) across the sediment-water interface were not detected, maximum diffusive fluxes (Fig. 7B) and depth-integrated concentrations (Fig. 8) of Fe^{2+} and org-Fe(III) in mid-slope sediments were the highest on the continental margin. Maximum diffusive fluxes of both Fe^{2+} and ΣH_2S peaked at St. 11 (665 m), whereas org-Fe(III) fluxes continued to increase with water depth over the mid-slope (Fig. 7B). Variations in maximum diffusive fluxes with depth differed slightly from the depth-integrated concentrations, which showed peaks in Fe^{2+} and org-Fe(III) concentrations around 600 m and an increase in ΣH_2S concentrations with depth (Fig. 8). Again, the lack of $FeS_{(aq)}$, the relatively low ΣH_2S concentrations (< 25 μM) in the depth profiles (Fig. 3), and the small changes in SO_4^{2-} and DIC concentrations with depth (Fig. 4) indicate that MSR was not significant in these mid-slope sediments. In turn, ΣPO_4^{3-} increased with sediment depth at both St. 5 and 11 (Fig. 4), and the highest diffusive ΣPO_4^{3-} fluxes were detected on the mid-slope (Fig. 7C), confirming increased rates of anaerobic respiration. The simultaneous production of both Fe^{2+} and org-Fe(III) directly below the OPD (9–12 mm) suggests active DIR in the first 15 to 60 mm of the mid-slope sediments (Fig. 3). However, the sharp decrease in Fe^{2+} and org-Fe(III) below 60 mm at St. 5, 40 mm at St. 11, and 15 mm at St. 13 indicate that MSR migrated upward in the sediment column and progressively compressed the DIR zone below the sediment-water interface as water column depth increased. Upward migration of MSR likely resulted from the increase input of organic material that accompanied the increase in Fe(III) oxides on the mid-slope relative to the upper-slope sediment (Fig. 5). This compression of the DIR zone may have increased the upward flux of org-Fe(III) as a function of water depth observed on the mid-slope (Fig. 7B). Incubations of St. 11 sediments confirm increased production of both dissolved Fe^{2+} and Fe(III) in the upper sediment of the mid-slope (Figs. 6 and S9). Unlike the upper-slope, however, depth-integrated Fe^{2+} production rates in mid-slope sediments were an order of magnitude lower than the maximum Fe^{2+} diffusive fluxes calculated from the depth profiles (Table 2). Although no significant changes in sulfate were observed in the incubations (Fig. S9), the differences between depth-integrated rates and diffusive fluxes could be due to precipitation of Fe^{2+} with sulfide which may be promoted on the mid-slope depocenter due to the increased organic matter available for anaerobic respiration. However, depth-integrated rates of dissolved Fe(III) production were larger than depth-integrated rates of Fe^{2+} production. Given the high reactivity of dissolved Fe(III) with sulfide (Taillefert et al., 2000a), these findings suggest that sulfate reduction was not significant in these sediments and that DIR may occur in the upper sediment layers on the mid-slope. Although a significant decrease in SO_4^{2-} concentrations with sediment depth was observed along the mid-slope of Cape Hatteras, sulfate did not significantly decrease in the top 50 cm of sediment in continental shelf, upper slope, and deep waters (Alperin et al., 1999; Jahnke and Jahnke, 2000; Thomas et al., 2002). Similarly, sulfate did not significantly decrease in the top 30 cm of sediment at mid-slope stations of Cape Lookout and Cape Fear (DeMaster et al., 1994; Schaff et al., 1992), supporting the results of this study.

4.4. Potential for benthic iron flux from passive continental margin sediments and global significance

The benthic iron flux in upwelling zones has been attributed either to a direct flux of Fe^{2+} in oxygen minimum zones, reoxidation and stabilization of iron under the form of dissolved Fe(III) complexes (Elrod et al., 2004; Lohan and Bruland, 2008; Noffke et al., 2012; Severmann et al., 2010), or resuspension of Fe(III) oxide particles (Bruland et al., 2001; Chase et al., 2005; Fitzwater et al., 2003; Johnson et al., 1999). Although the measurements obtained in this study did not detect any benthic flux at the sediment-water interface, the millimeter resolution and the unique speciation capability of voltammetric measurements demonstrated that Fe^{2+} and org-Fe(III) reached the oxic zone (as determined by the OPD) on the mid-slope (Fig. 3). At four of the five mid-slope stations, diffusive Fe^{2+} flux into the oxic zone were non-zero (Table 3) resulting in an average upward flux of

Table 3
Maximum diffusive fluxes of Fe^{2+} and organic-Fe(III) complexes compared to their diffusive fluxes into the oxic zone at all mid-slope stations (their diffusive fluxes across the sediment-water interface were below detection limit). For comparison, maximum dissolved sulfide fluxes are also provided. Diffusive fluxes of Fe^{2+} and ΣH_2S are in mmol m^{-2} day^{-1}, whereas the org-Fe(III) diffusive flux is in nA m^{-2} day^{-1}.

Station	Depth (m)	Maximum diffusive flux			Diffusive flux into oxic zone	
		Fe^{2+}	Org-Fe(III)	ΣH_2S	Fe^{2+}	Org-Fe(III)
12	580	−0.44 ± 0.02	−0.48 ± 0.09	−0.0034 ± 0.0006	0	0
5	589	−0.95 ± 0.4	−0.92 ± 0.2	−0.012 ± 0.003	−0.63 ± 0.2	−0.82 ± 0.2
10	596	−1.01 ± 0.4	−0.89 ± 0.1	−0.024 ± 0.004	−1.01 ± 0.4	0
11	665	−1.22 ± 0.3	−2.46 ± 0.3	−0.087 ± 0.01	−1.05 ± 0.4	−1.64 ± 0.8
13	840	−1.11 ± 0.3	−5.08 ± 0.6	−0.10 ± 0.01	−1.11 ± 0.3	−5.08 ± 0.6

-0.95 ± 0.2 mmol Fe^{2+} m^{-2} day^{-1}, which is the same order of magnitude, although slightly higher, than the benthic Fe^{2+} fluxes of -0.29 mmol Fe^{2+} m^{-2} day^{-1} observed between 638 and 905 m (Elrod et al., 2004) and -0.57 mmol Fe^{2+} m^{-2} day^{-1} at 900 m water depth (Severmann et al., 2010) in oxygen minimum zones along the California coast. Depth-integrated rates of Fe^{2+} production observed in the surface sediment incubations of St. 11 (Table 2) further indicate that sedimentary production of Fe^{2+} in mid-slope sediments with fully oxygenated bottom waters not exposed to upwelling is similar to oxygen limited upwelling zones. Despite similar Fe^{2+} production rates, however, oxidation by dissolved O_2 decreases the flux of Fe^{2+} into the overlying waters significantly, as demonstrated previously (Noffke et al., 2012; Dale et al., 2015). A close examination of the mid-slope depth profiles indeed confirms that Fe^{2+} did not reach the sediment-water interface (Fig. S10). In addition, DOU varied concomitantly with maximum diffusive fluxes of Fe^{2+} across the continental slope (Fig. 7A,B), providing insight into the mechanism of O_2 consumption.

Sedimentary Fe^{2+} oxidation in the presence of organic ligands may promote the formation of soluble org-Fe(III) compounds in the oxic zone of non-upwelling mid-slope depocenters such as that found off the coast of Cape Lookout (Fig. S10). Unfortunately, voltammetric interference of dissolved oxygen prevents detection of org-Fe(III) in fully oxic waters (Luther et al., 2008). In addition, the complexes detected must be of small sizes (< 5 nm) to diffuse and react at the electrode surface, such that larger complexes may remain undetected (Taillefert et al., 2000a). Despite these analytical drawbacks, a diffusive org-Fe(III) flux into the oxic zone was observed at three of the five mid-slope stations (Table 3), and although these values are reported in normalized voltammetric signals (nA) which cannot be quantified, the detection of these species suggests the potential release of a bioavailable form of iron to the overlying waters. The production of 0.27 ± 0.004 mmol of dissolved Fe(III) m^{-2} day^{-1} in anaerobic sediment incubations from St. 11 is greater than the depth-integrated Fe^{2+} production rate (Table 3) and confirms the production of these species in surface sediments. Complexation by organic ligands during the upward diffusion and oxidation of Fe^{2+} in the oxic sediment layers may even result in increased concentrations of dissolved Fe(III) which cannot be accounted for in the anaerobic incubations.

Although present iron cycling models require further improvements (Tagliabue et al., 2017), dissolved iron input of 8.9×10^{10} mol yr^{-1} based on a mean shelf flux of 4.3 μmol Fe^{2+} m^{-2} day^{-1} extrapolated over the global shelf area (Elrod et al., 2004) has been widely used in biogeochemical models (Moore et al., 2004; Muglia et al., 2017; Raiswell et al., 2006). Interestingly, the iron input from continental slopes has been mostly overlooked in these models. The present work suggests that a potentially significant fraction of complexed iron may be released from mid-slope sediments despite the fully oxygenated waters and lack of intense upwelling and that this supply of dissolved Fe(III) to the overlying waters should be accounted for in future ocean models.

Based on the Cape Lookout slope surface area (Fig. 1), mid-slope depocenters compose approximately 12% (3.9×10^{12} m^2) of the global continental slope surface area (3.25×10^{13} m^2 (Walsh, 1989)). Although the global mid-slope surface area will have to be revaluated once other mid-slopes have been investigated, extrapolation of the benthic Fe^{2+} flux determined on the California mid-slope (-0.289 mmol m^{-2} day^{-1} (Elrod et al., 2004), -0.568 mmol m^{-2} day^{-1} (Severmann et al., 2010)) over the global surface area of mid-slope depocenters results in a global Fe^{2+} input of $4.1–8.1 \times 10^{11}$ mol yr^{-1}, demonstrating the importance of these sediments in the global supply of iron to the ocean. Indeed, recent global estimates, which did not capture the extreme fluxes observed in mid-slope sediments, report input from total slope sediments of just 0.37×10^{11} mol yr^{-1} (Dale et al., 2015). Due to the rapid oxidation of Fe^{2+} in fully oxygenated waters, extrapolation of the diffusive Fe^{2+} fluxes into the oxic zone determined in mid-slope sediments off Cape Lookout would likely result in an overestimation of iron input to the ocean. Sediment incubations, which support the measured diffusive Fe^{2+} fluxes, also enable quantification of dissolved Fe(III) production. The depth-integrated dissolved Fe(III) production rates from the Cape Lookout mid-slope sediment incubations (St. 11 in Table 2) conducted in anaerobic conditions represent a conservative estimate of dissolved Fe(III) fluxes to the overlying waters, as formation of org-Fe(III) during oxidation of Fe^{2+} in the presence of O_2 at the sediment-water interface is not accounted for in these rates. Additionally, anaerobic incubations may, to some extent, promote MSR and production of ΣH_2S, which rapidly reduces org-Fe(III) (Taillefert et al., 2000a), thus resulting in a decrease in net rates of org-Fe(III) production in these incubations. Although sediment incubations do likely not reflect the actual benthic flux generated at the sediment-water interface, these incubations can help evaluate whether the benthic iron flux from passive continental margins is negligible or should be investigated further. Extrapolation of the dissolved Fe(III) flux from these incubations results in a global input of 3.8×10^{11} mol yr^{-1} to the ocean. This global input of dissolved Fe (III) from mid-slope sediments rival global estimates of iron inputs derived from aerosols ($1–6 \times 10^{11}$ mol Fe yr^{-1} (Fung et al., 2000; Jickells and Spokes, 2001)), rivers ($1.5–26 \times 10^9$ mol Fe yr^{-1} (Martin and Meybeck, 1979; Poulton and Raiswell, 2002)), and hydrothermal vents (0.9×10^9 mol Fe yr^{-1} (Tagliabue et al., 2010)). Recent biogeochemical models indicate that the subsurface dissolved iron maximum detected on GEOTRACES transects in the western Atlantic may be dependent on iron complexation with organic ligands and suggest that continental shelves may be an important iron source in the Southern Atlantic (Pham and Ito, 2018). The results of this study provide evidence that passive continental slope sediments may represent a source of complexed iron to the ocean and suggest that benthic iron fluxes and the speciation of dissolved iron crossing the sediment-water interface should be quantified in future studies of continental slope sediments.

5. Conclusion

In this study, the diffusive flux of iron and its speciation in the sediment was determined along a transect across the continental shelf and slope near Cape Lookout, North Carolina to investigate the potential for passive continental margin sediments without large upwelling events or

riverine input to provide dissolved iron to the ocean. Large maximum diffusive fluxes of both dissolved Fe^{2+} and org-Fe(III) complexes over the mid-slope, backed up by depth-integrated rates of dissolved Fe^{2+} and Fe(III) determined from sediment incubations, demonstrate increased microbial activity in mid-slope depocenters relative to shelf sediments. The production of dissolved Fe(III) is likely regulated by a combination of aerobic oxidation in the presence of natural organic ligands near the sediment-water interface, DIR deep in the sediments, and chemical oxidation of Fe(II) complexed to natural organic ligands across the sediment column. Although the diffusive fluxes of Fe^{2+} and org-Fe(III) across the sediment-water were not detected, diffusive flux org-Fe(III) into the oxic zone of these sediments (< 1 cm below the sediment-water interface) along with production of dissolved Fe(III) in sediment slurry incubations suggest that complexation of Fe(III) in these sediments may contribute to the stabilization and potential transport of dissolved iron into oxygenated deep ocean waters. Extrapolation of the estimated sedimentary flux from the Cape Lookout mid-slope depocenter to the global ocean indicates that this iron flux may rival global estimates of iron inputs derived from aerosols, rivers, and hydrothermal vents. These findings suggest that passive margins and continental slope sediments that are generally overlooked in global estimates may generate a significant flux of iron across the sediment water interface, thus warranting the need for measurement of benthic iron fluxes and dissolved iron speciation in these environments.

Supplementary data to this article can be found online at https://doi.org/10.1016/j.marchem.2020.103750.

Acknowledgments

We would like to thank the captain and crew of the R/V Savannah for their invaluable help during the different cruises. We would also like to thank the Editor and two anonymous reviewers for their constructive comments on previous versions of this paper. The National Science Foundation (OCE-0851156 and OCE-1438648) funded this research.

References

Aller, R.C., 1982. The effects of macrobenthos on chemical properties of marine sediment and overlaying water. In: McCall, P.L., Tevesz, M.J.S. (Eds.), Animal-sediment Relations. Plenum Press, New York, pp. 53–101.
Aller, J.Y., Aller, R.C., Green, M.A., 2002. Benthic faunal assemblages and carbon supply along the continental shelf/shelf break-slope off Cape Hatteras, North Carolina. Deep Sea Res. II 49, 4599–4625.
Alperin, M.J., et al., 1999. Benthic fluxes and porewater concentration profiles of dissolved organic carbon in sediments from the North Carolina continental slope. Geochim. Cosmochim. Acta 63 (3–4), 427–448.
Alperin, M.J., Suayah, I.B., Benninger, L.K., Martens, C.S., 2002. Modern organic carbon burial fluxes, recent sedimentation rates, and particle mixing rates from the upper continental slope near Cape Hatteras, North Carolina (USA). Deep-Sea Res. II Top. Stud. Oceanogr. 49 (20), 4645–4665.
Amante, C., Eakins, B.W., 2009. ETOPO1 1 arc-minute global relief model: procedures, data sources and analysis. In: NOAA Technical Memorandum NESDIS NGDC-24. National Geophysical Data Center, NOAA.
Anderson, R.F., Rowe, G.T., Kemp, P.F., Trumbores, S., Biscaye, P.E., 1994. Carbon budget for the mid-slope depocenter of the middle Atlantic bight. Deep-Sea Res. II Top. Stud. Oceanogr. 41 (2), 669–703.
Anschutz, P., Zhong, S.J., Sundby, B., Mucci, A., Gobeil, C., 1998. Burial efficiency of phosphorus and the geochemistry of iron in continental margin sediments. Limnol. Oceanogr. 43 (1), 53–64.
Archer, D., Devol, A., 1992. Benthic oxygen fluxes on the Washington shelf and slope: A comparison of in situ microelectrode and chamber flux measurements. Limonl Oceanogr 37 (3), 614–629.
de Baar, H., et al., 1990. On Iron Limitation of the Southern Ocean: Experimental Observations in the Weddell and Scotia Sea. 65 (105–122 pp).
Barrett, J.R., 1965. Subsurface currents off Cape Hatteras. Deep-Sea Res. Oceanogr. Abstr. 12 (2), 173–184.
Beckler, J.S., Nuzzio, D.B., Taillefert, M., 2014. Development of single-step liquid chromatography methods with ultraviolet detection for the measurement of inorganic anions in marine waters. Limnol. Oceanogr. Methods 12, 563–576.
Beckler, J.S., Jones, M.E., Taillefert, M., 2015. The origin, composition, and reactivity of dissolved iron(III) complexes in coastal organic- and iron-rich sediments. Geochim. Cosmochim. Acta 152, 72–88.
Beckler, J.S., Kiriazis, N., Rabouille, C., Stewart, F.J., Taillefert, M., 2016. Importance of microbial iron reduction in deep sediments of river-dominated continental-margins.
Behrenfeld, M.J., Kolber, Z.S., 1999. Widespread iron limitation of phytoplankton in the South Pacific Ocean. Science 283 (5403), 840–843.
Berelson, W., et al., 2003. A time series of benthic flux measurements from Monterey Bay, CA. Cont. Shelf Res. 23 (5), 457–481.
van den Berg, C.M.G., 1995. Evidence for organic complexation of iron in seawater. Mar. Chem. 50 (1), 139–157.
Bhatia, M.P., et al., 2013. Greenland meltwater as a significant and potentially bioavailable source of iron to the ocean. Nat. Geosci. 6 (4), 274–278.
Biscaye, P.E., Anderson, R.F., Deck, B.L., 1988. Fluxes of particles and constituents to the eastern United States continental slope and rise: SEEP—I. Cont. Shelf Res. 8 (5), 855–904.
Blair, N.E., Plaia, G.R., Boehme, S.E., DeMaster, D.J., Levin, L.A., 1994. The remineralization of organic carbon on the North Carolina continental slope. Deep-Sea Res. II Top. Stud. Oceanogr. 41 (4), 755–766.
Blake, J.A., Grassle, J.F., 1994. Benthic community structures on the U.S. South Atlantic slope off the Carolinas: spatial heterogenetiy in a current-dominated system. Deep-Sea Res. II 41 (4), 835–874.
Blake, J.A., Hilbig, B., 1994. Dense infaunal assemblages on the continental slope off Cape Hatteras, North Carolina. Deep-Sea Research II 41, 875–899.
Blake, J.A., et al., 1985. Study of Biological Processes on the U.S. South Atlantic Slope and Rise. Phase 1. Benthic Characterization Study. Final Report, U.S. Department of the Interior, Minerals Management Service, Washington, DC.
Blake, J.A., et al., 1987. Study of Biological Processes on the U.S. South Atlantic Slope and Rise. Phase 2. Final Report, U.S. Department of the Interior, Minerals Management Service, Washington, DC.
Boudreau, B.P., 1997. Diagenetic Models and their Implementation: Modeling Transport and Reactions in Aquatic Sediments. Springer-Verlag.
Boyle, E.A., Edmond, J.M., Sholkovitz, E.R., 1977. Mechanism of iron removal in estuaries. Geochim. Cosmochim. Acta 41 (9), 1313–1324.
Brendel, P.J., Luther, G.W., 1995. Development of a gold amalgam voltammetric mirroelectrode for the determination of dissolved Fe, Mn, O2, and S(-II) in porewater of marine and fresh-water sediments. Environ. Sci. Technol. 29 (3), 751–761.
Bristow, G., Taillefert, M., 2008. VOLTINT: a Matlabg (R)-based program for semi-automated processing of geochemical data acquired by voltammetry. Comput. Geosci. 34 (2), 153–162.
Bruland, K.W., Rue, E.L., Smith, G.J., 2001. Iron and macronutrients in California coastal upwelling regimes: implications for diatom blooms. Limnol. Oceanogr. 46 (7), 1661–1674.
Buck, K.N., Lohan, M.C., Berger, C.J.M., Bruland, K.W., 2007. Dissolved iron speciation in two distinct river plumes and an estuary: implications for riverine iron supply. Limnol. Oceanogr. 52 (2), 843–855.
Burdige, D.J., Alperin, M.J., Homstead, J., Martens, C.S., 1992. The role of benthic fluxes of dissolved organic carbon in oceanic and sedimentary carbon cycling. Geophys. Res. Lett. 19 (18), 1851–1854.
Canfield, D.E., 1989. Sulfate reduction and oxic respiration in marine sediments: implications for organic carbon preservation in euxinic environments. Deep Sea Res. A 36 (1), 121–138.
Carpenter, R., 1987. Has man altered the cycling of nutrients and organic C on the Washington continental shelf and slope? Deep Sea Res. A 34 (5), 881–896.
Cerame-Vivas, M.J., Gray, I.E., 1966. The distributional pattern of benthic invertebrates of the continental shelf off North Carolina. Ecology 47 (2), 260–270.
Chase, Z., et al., 2005. Manganese and iron distributions off Central California influenced by upwelling and shelf width. Mar. Chem. 95 (3), 235–254.
Chen, M., Wang, W.X., Guo, L., 2004. Phase partitioning and solubility of iron in natural seawater controlled by dissolved organic matter. Glob. Biogeochem. Cycles 18 (4).
Coale, K.H., et al., 1996. A massive phytoplankton bloom induced by an ecosystem-scale iron fertilization experiment in the equatorial Pacific Ocean. Nature 383 (6600), 495–501.
Cornel, P.K., Summers, R.S., Roberts, P.V., 1986. Diffusion of humic-acid in dilute aqueous-solution. J. Colloid Interface Sci. 110 (1), 149–164.
Csanady, G.T., 1990. Physical basis of coastal productivity: the SEEP and MASAR experiments. EOS 71 (36), 1060–1065.
Csanady, G.T., Hamilton, P., 1988. Circulation of slopewater. Cont. Shelf Res. 8 (5), 565–624.
Dale, A.W., et al., 2015. A revised global estimate of dissolved iron fluxes from marine sediments. Glob. Biogeochem. Cycles 29 (5), 691–707.
DeMaster, D.J., Pope, R.H., Levin, L.A., Blair, N.E., 1994. Biological mixing intensity and rates of organic carbon accumulation in North Carolina slope sediments. Deep-Sea Res. II Top. Stud. Oceanogr. 41 (4), 735–753.
DeMaster, D.J., et al., 2002. Deposition of bomb 14C in continental slope sediments of the mid-Atlantic bight: assessing organic matter sources and burial rates. Deep-Sea Res. II Top. Stud. Oceanogr. 49 (20), 4667–4685.
Diaz, R.J., Cutter, G.R., Rhoads, D.C., 1994. The importance of bioturbation to continental slope sediment structure and benthic processes off Cape Hatteras, North Carolina. Deep-Sea Res. II Top. Stud. Oceanogr. 41 (4), 719–734.
Dickson, A.G., 1993. pH buffers for sea water media based on the total hydrogen ion concentration scale. Deep-Sea Res. I Oceanogr. Res. Pap. 40 (1), 107–118.
Elrod, V.A., Berelson, W.M., Coale, K.H., Johnson, K.S., 2004. The flux of iron from continental shelf sediments: a missing source for global budgets. Geophys. Res. Lett. 31 (12).
Esch, M.E.S., Shull, D.H., Devol, A.H., Moran, S.B., 2013. Regional patterns of bioturbation and iron and manganese reduction in the sediments of the southeastern Bering Sea. Deep-Sea Res. II 94, 80–94.
Falkowski, P.G., Barber, R.T., Smetacek, V., 1998. Biogeochemical controls and feedbacks on ocean primary production. Science 281 (5374), 200–206.
Fennessey, C.M., Jones, M.E., Taillefert, M., DiChristina, T.J., 2010. Siderophores are not

involved in Fe(III) Solubilization during anaerobic Fe(III) respiration by Shewanella oneidensis MR-1. Appl. Environ. Microbiol. 76 (8), 2425–2432.
Fitzwater, S.E., et al., 2003. Iron, nutrient and phytoplankton biomass relationships in upwelled waters of the California coastal system. Cont. Shelf Res. 23 (16), 1523–1544.
Friedl, G., Dinkel, C., Wehrli, B., 1998. Benthic fluxes of nutrients in the northwestern Black Sea. Mar. Chem. 62 (1), 77–88.
Friedrich, J., et al., 2002. Benthic nutrient cycling and diagenetic pathways in the North-Western Black Sea. Estuar. Coast. Shelf Sci. 54 (3), 369–383.
Fornes, W.L., DeMaster, D.J., Levin, L.A., Blair, N.E., 1999. Bioturbation and particle transportation in Carolina slope sediments: A radiochemical approach. Journal of Marine Research. 57, 335–355.
Fung, I.Y., et al., 2000. Iron supply and demand in the upper ocean. Glob. Biogeochem. Cycles 14 (1), 281–295.
Gerringa, L.J.A., et al., 2007. Kinetic study reveals weak Fe-binding ligand, which affects the solubility of Fe in the Scheldt estuary. Mar. Chem. 103 (1), 30–45.
Gledhill, M., Van Den Berg, C.M.G., 1994. Determination of complexation of iron(III) with natural organic complexing ligands in seawater using cathodic stripping voltammetry. Mar. Chem. 47 (1), 41–54.
Glud, R.N., 2008. Oxygen dynamics of marine sediments. Mar. Biol. Res. 4 (4), 243–289.
Gooday, A.J., Hughes, J.A., Levin, L.A., 2001. The foraminiferan from three North Carolina (USA) slope sites with contrasting carbon flux: a comparison with the metazoan macrofauna. Deep-Sea Res. I. 48, 1709–1739.
Green, M.A., Aller, R.C., Cochran, J.K., Lee, C., Aller, J.Y., 2002. Bioturbation in shelf/slope sediments off Cape Hatteras North Carolina: the use of 234Th, Chl-a, and Br- to evaluate rates of particle and solute transport. Deep-Sea Research II 49, 4627–4644.
Hall, P.J., Aller, R.C., 1992. Rapid, small-volume, flow injection analysis for SCO2, and NH4+ in marine and freshwaters. Limnol. Oceanogr. 37 (5), 1113–1119.
Harris, P.T., Macmillan-Lawler, M., Rupp, J., Baker, E.K., 2014. Geomorphology of the oceans. Mar. Geol. 352, 4–24.
Heip, C.H.R., et al., 1995. Production and consumption of biological particles in temperate tidal estuaries. Oceanogr. Mar. Biol. Annu. Rev. 33, 1–149.
Honjo, S., Francois, R., Manganini, S., Dymond, J., Collier, R., 2000. Particle fluxes to the interior of the Southern Ocean in the Western Pacific sector along 170 degrees W. Deep-Sea Res. II 47 (15–16), 3521–3548.
Jahnke, R.A., Jahnke, D.B., 2000. Rates of C, N, P and Si recycling and denitrification at the US mid-Atlantic continental slope depocenter. Deep-Sea Res. I 47 (8), 1405–1428.
Jahnke, R.A., et al., 2005. Organic matter remineralization and porewater exchange rates in permeable South Atlantic bight continental shelf sediments. Cont. Shelf Res. 25 (12), 1433–1452.
Janowitz, G.S., Pietrafesa, L.J., 1980. A model and observations of time-dependent upwelling over the mid-shelf and slope. J. Phys. Oceanogr. 10 (10), 1574–1583.
Jickells, T., Spokes, L., 2001. Atmospheric iron inputs to the oceans. In: Turner, D., Hunter, K. (Eds.), Biogeochemistry of Iron in Seawater. Wiley, New York.
Jickells, T.D., et al., 2005. Global iron connections between desert dust, ocean biogeochemistry, and climate. Science 308 (5718), 67–71.
Johnson, T.C., 1989. Hydrography and sedimentation on the continental slope and rise off north and South Carolina. In: North Carolina Coastal Oceanography Symposium. National Undersea Research Program 89-2, pp. 151–172.
Johnson, K.S., Gordon, R.M., Coale, K.H., 1997. What controls dissolved iron concentrations in the world ocean? Mar. Chem. 57 (3–4), 137–161.
Johnson, K.S., Chavez, F.P., Friederich, G.E., 1999. Continental-shelf sediment as a primary source of iron for coastal phytoplankton. Nature 398 (6729), 697–700.
Jones, M.E., Fennessey, C.M., DiChristina, T.J., Taillefert, M., 2010. Shewanella oneidensis MR-1 mutants selected for their inability to produce soluble organic-Fe(III) complexes are unable to respire Fe(III) as anaerobic electron acceptor. Environ. Microbiol. 12 (4), 938–950.
Jones, M.E., Beckler, J.S., Taillefert, M., 2011. The flux of soluble organic-iron(III) complexes from sediments represents a source of stable iron(III) to estuarine waters and to the continental shelf. Limnol. Oceanogr. 56 (5), 1811–1823.
Kemp, P.F., 1994. Microbial carbon utilization on the continental shelf and slope during the SEEP-II experiment. Deep-Sea Res. II Top. Stud. Oceanogr. 41 (2), 563–581.
Kemp, W.M., Sampou, P.A., Garber, J., Tuttle, J., Boynton, W.R., 1992. Seasonal depletion of oxygen from bottom waters of Chesapeake Bay: roles of benthic and planktonic respiration and physical exchange processes. Mar. Ecol. Prog. Ser. 85 (1–2), 137–152.
Kolber, Z.S., et al., 1994. Iron limitation of Phytoplanton photosynthesis in teh equatorial Pacific Ocean. Nature 371 (6493), 145–149.
Kostka, J.E., Luther, G.W., 1994. Partitioning and speciation of solid phase iron in salt-marsh sediments. Geochim. Cosmochim. Acta 58 (7), 1701–1710.
Lam, P.J., Bishop, J.K.B., 2008. The continental margin is a key source of iron to the HNLC North Pacific Ocean. Geophys. Res. Lett. 35 (7).
Lam, P.J., et al., 2006. Wintertime phytoplankton bloom in the subarctic Pacific supported by continental margin iron. Glob. Biogeochem. Cycles 20 (1).
Levin, L., Blair, N., DeMaster, D., Plaia, G., Fornes, W., Martin, C., Thomas, C., 1997. Rapid subduction of organic matter by maldanid polychaetes on the North Carolina slope. J. Mar. Res. 55, 595–611.
Liu, X.W., Millero, F.J., 2002. The solubility of iron in seawater. Mar. Chem. 77 (1), 43–54.
Lohan, M.C., Bruland, K.W., 2008. Elevated Fe(II) and dissolved Fe in hypoxic shelf waters off Oregon and Washington: an enhanced source of Iron to coastal upwelling regimes. Environ. Sci. Technol. 42 (17), 6462–6468.
Luther, G.W., Kostka, J.E., Church, T.M., Sulzberger, B., Stumm, W., 1992. Seasonal iron cycling in the salt-marsh sedimentary environment - the importance of ligand complexes with Fe(II) and Fe(III) in the dissolution of Fe(III) minerals and pyrite respectively. Mar. Chem. 40 (1–2), 81–103.
Luther, G.W., et al., 2008. Use of voltammetric solid-state (micro)electrodes for studying biogeochemical processes: laboratory measurements to real time measurements with an in situ electrochemical analyzer (ISEA). Mar. Chem. 108 (3–4), 221–235.
Macrellis, H.M., Trick, C.G., Rue, E.L., Smith, G., Bruland, K.W., 2001. Collection and detection of natural iron-binding ligands from seawater. Mar. Chem. 76 (3), 175–187.
Marinelli, R.L., Jahnke, R.A., Craven, D.B., Nelson, J.R., Eckman, J.E., 1998. Sediment nutrient dynamics on the South Atlantic bight continental shelf. Limnol. Oceanogr. 43 (6), 1305–1320.
Martin, J.H., 1990. Glacial-interglacial CO2 change: the iron hypothesis. Paleoceanography 5 (1), 1–13.
Martin, J.H., Fitzwater, S.E., 1988. Iron-deficiency limits phytoplankton growth in the northeast pacific subarctic. Nature 331 (6154), 341–343.
Martin, J.M., Meybeck, M., 1979. Elemental mass-balance of material carried by major world rivers. Mar. Chem. 7 (3), 173–206.
McGregor, B., 1984. Resolution: a key to better understanding continental slope and rise processes. In: U.S. Atlantic Continental Margin. Ocean Technology Conference, Paper 4722, 16th Annual OTC, pp. 111–118.
Mellor, C.A., Paull, C.K., 1994. Sea beam bathymetry of the Manteo 467 lease block off Cape Hatteras, North Carolina. Deep-Sea Res. II Top. Stud. Oceanogr. 41 (4), 711–718.
Millero, F.J., 1998. Solubility of Fe(III) in seawater. Earth Planet. Sci. Lett. 154 (1), 323–329.
Millero, F.J., Yao, W., Aicher, J., 1995. The speciation of Fe(II) and Fe(III) in natural waters. Mar. Chem. 50 (1), 21–39.
Milliman, J.D., 1994. Organic matter content in U.S. Atlantic continental slope sediments: decoupling the grain-size factor. Deep-Sea Res. II Top. Stud. Oceanogr. 41 (4), 797–808.
Milliman, J.D., Pilkey, O.H., Ross, D.A., 1972. Sediments of the continental margin off the eastern United States. GSA Bull. 83 (5), 1315–1334.
Moore, J.K., Doney, S.C., Glover, D.M., Fung, I.Y., 2002. Iron cycling and nutrient-limitation patterns in surface waters of the World Ocean. Deep-Sea Res. II 49 (1–3), 463–507.
Moore, J.K., Doney, S.C., Lindsay, K., 2004. Upper Ocean ecosystem dynamics and iron cycling in a global three-dimensional model. Glob. Biogeochem. Cycles 18 (4).
Muglia, J., Somes, C.J., Nickelsen, L., Schmittner, A., 2017. Combined effects of atmospheric and seafloor iron fluxes to the Glacial Ocean. Paleoceanography 32 (11), 1204–1218.
Murphy, J., Riley, J.P., 1962. A modified single solution method for determination of phosphate in natural water. Anal. Chim. Acta 26 (1), 31.
Murray, J.W., Kuivila, K.M., 1990. Organic matter diagenesis in the Northeast Pacific: transition from aerobic red clay to suboxic hemipelagic sediments. Deep Sea Res. A 37 (1), 59–80.
Nevin, K.P., Lovley, D.R., 2002. Mechanisms for accessing insoluble Fe(III) oxide during dissimilatory Fe(III) reduction by Geothrix fermentans. Appl. Environ. Microbiol. 68 (5), 2294–2299.
Noffke, A., et al., 2012. Benthic iron and phosphorus fluxes across the Peruvian oxygen minimum zone. Limnol. Oceanogr. 57 (3), 851–867.
Pedersen, T.F., Shimmield, G.B., P, N.B., 1992. Lack of enhanced preservation of organic matter in sediments under the oxygen minimum on the Oman Margin. Geochim. Cosmochim. Acta 56 (1), 545–551.
Perdue, E.M., Beck, K.C., Helmut Reuter, J., 1976. Organic complexes of iron and aluminium in natural waters. Nature 260, 418.
Pham, A.L.D., Ito, T., 2018. Formation and maintenance of the GEOTRACES subsurface-dissolved Iron maxima in an ocean biogeochemistry model. Glob. Biogeochem. Cycles 32 (6), 932–953.
Pietrafesa, L.J., Janowitz, G.S., Wittman, P.A., 1985. Physical Oceanographic Processes in the Carolina Capes, Oceanography of the Southeastern U.S. Continental Shelf. American Geophysical Union, pp. 23–32.
Popenoe, P., 1980. Single-channel seismic-reflection profiles collected on the northern Blake plateau, 29 September to 19 October 1978. U.S. Geol. Surv. Open-File Rep. 4, 80–1256.
Popenoe, P., Coward, E.L., Cashman, K.V., 1982. A Regional Assessment of Potential Environmental Hazards to and Limitations on Petroleum Development of the Southeastern United States Atlantic Continental Shelf, Slope, and Rise, Offshore North Carolina. pp. 82–136.
Poulton, S.W., Raiswell, R., 2002. The low-temperature geochemical cycle of iron: from continental fluxes to marine sediment deposition. Am. J. Sci. 302 (9), 774–805.
Pratt, R.M., 1966. The Gulf stream as a graded river. Limnol. Oceanogr. 11, 60–67.
Premuzic, E.T., Benkovitz, C.M., Gaffney, J.S., Walsh, J.J., 1982. The nature and distribution of organic matter in the surface sediments of world oceans and seas. Org. Geochem. 4 (2), 63–77.
Raiswell, R., et al., 2006. Contributions from glacially derived sediment to the global iron (oxyhydr)oxide cycle: implications for iron delivery to the oceans. Geochim. Cosmochim. Acta 70 (11), 2765–2780.
Raiswell, R., Benning, L.G., Tranter, M., Tulaczyk, S., 2008. Bioavailable iron in the Southern Ocean: the significance of the iceberg conveyor belt. Geochem. Trans. 9.
Rhoads, D.C., Hecker, B., 1994. Processes on the continental slope off North Carolina with special reference to the Cape Hatteras region. Deep-Sea Res. II Top. Stud. Oceanogr. 41 (4), 965–980.
Richardson, P.L., 1977. On the crossover between the Gulf stream and the Western boundary undercurrent. Deep-Sea Res. 24 (2), 139–159.
Roden, E.E., Sobolev, D., Glazer, B., Luther, G.W., 2004. Potential for microscale bacterial Fe redox cycling at the aerobic-anaerobic Interface. Geomicrobiol J. 21 (6), 379–391.
Rowe, G.T., Menzies, R.J., 1968. Deep bottom currents off the coast of North Carolina. Deep-Sea Res. Oceanogr. Abstr. 15 (6), 711–719.
Rowe, G.T., Boland, G.S., Phoel, W.C., Anderson, R.F., Biscaye, P.E., 1994. Deep-sea floor

respiration as an indication of lateral input of biogenic detritus from continental margins. Deep-Sea Res. II Top. Stud. Oceanogr. 41 (2), 657–668.
Rozan, T.F., et al., 2002. Iron-sulfur-phosphorus cycling in the sediments of a shallow coastal bay: implications for sediment nutrient release and benthic macroalgal blooms. Limnol. Oceanogr. 47 (5), 1346–1354.
Rue, E.L., Bruland, K.W., 1995. Complexation of iron(III) by natural organic ligands in the central North Pacific as determined by a new competitive ligand equilibration/adsorptive cathodic stripping voltammetric method. Mar. Chem. 50 (1), 117–138.
Rue, E.L., Bruland, K.W., 1997. The role of organic complexation on ambient iron chemistry in the equatorial Pacific Ocean and the response of a mesoscale iron addition experiment. Limnol. Oceanogr. 42 (5), 901–910.
Schaff, T., Blair, N., Demaster, D., Pope, R., Boehme, S., 1992. Spatial heterogeneity of benthos on the Carolina continental slope: large (100km)-scale variation. Mar. Ecol. Prog. Series 88 (2–3), 143–160.
Severmann, S., McManus, J., Berelson, W.M., Hammond, D.E., 2010. The continental shelf benthic iron flux and its isotope composition. Geochim. Cosmochim. Acta 74 (14), 3984–4004.
Smith, K.L., Carlucci, A.F., Jahnke, R.A., Craven, D.B., 1987. Organic carbon mineralization in the Santa Catalina Basin: benthic boundary layer metabolism. Deep Sea Res. A 34 (2), 185–211.
Sobolev, D., Roden, E.E., 2001. Suboxic deposition of ferric iron by bacteria in opposing gradients of Fe(II) and oxygen at circumneutral pH. Appl. Environ. Microbiol. 67 (3), 1328–1334.
Stefánsson, U., Atkinson, L.P., Bumpus, D.F., 1971. Hydrographic properties and circulation of the North Carolina shelf and slope waters. Deep-Sea Res. Oceanogr. Abstr. 18 (4), 383–420.
Stookey, L.L., 1970. Ferrozine - a new spectrophotometric reagent for iron. Anal. Chem. 42 (7), 779.
Tagliabue, A., et al., 2010. Hydrothermal contribution to the oceanic dissolved iron inventory. Nat. Geosci. 3, 252.
Tagliabue, A., et al., 2017. The integral role of iron in ocean biogeochemistry. Nature 543, 51.
Taillefert, M., Bono, A.B., Luther, G.W., 2000a. Reactivity of freshly formed Fe(III) in synthetic solutions and (pore)waters: voltammetric evidence of an aging process. Environ. Sci. Technol. 34 (11), 2169–2177.
Taillefert, M., Luther, G.W., Nuzzio, D.B., 2000b. The application of electrochemical tools for in situ measurements in aquatic systems. Electroanalysis 12 (6), 401–412.
Taillefert, M., et al., 2007. Shewanella putrefaciens produces an Fe(III)-solubilizing organic ligand during anaerobic respiration on insoluble Fe(III) oxides. J. Inorg. Biochem. 101 (11 − 12), 1760–1767.
Tercier-Waeber, M.L., Taillefert, M., 2008. Remote in situ voltammetric techniques to characterize the biogeochemical cycling of trace metals in aquatic systems. J. Environ. Monit. 10 (1), 30–54.
Thomas, C.J., et al., 2002. Organic carbon deposition on the North Carolina continental slope off Cape Hatteras (USA). Deep-Sea Res. II Top. Stud. Oceanogr. 49 (20), 4687–4709.
Ullman, W.J., Aller, R.C., 1982. Diffusion coefficients in nearshore marine sediments1. Limnol. Oceanogr. 27 (3), 552–556.
Walsh, J.J., 1989. How much shelf production reaches the deep sea? In: Berger, W.H., Smetacek, V., Wefer, G. (Eds.), Productivity of the Ocean: Present and Past. Wiley, Dahlem Konferenzen, pp. 175–191.
Walsh, J.J., et al., 1985. Organic storage of CO2 on the continental slope off the mid-Atlantic bight, the southeastern Bering Sea, and the Peru coast. Deep Sea Res. A 32 (7), 853–883.
Walsh, J.J., Biscaye, P.E., Csanady, G.T., 1988. The 1983–1984 shelf edge exchange processes (SEEP)—I experiment: hypotheses and highlights. Cont. Shelf Res. 8 (5), 435–456.
Wu, J.F., Luther, G.W., 1994. Size-fractionated iron concentrations in the water column of the western North-Atlantic Ocean. Limnol. Oceanogr. 39 (5), 1119–1129.
Wu, J., Boyle, E., Sunda, W., Wen, L.-S., 2001. Soluble and colloidal Iron in the oligotrophic North Atlantic and North Pacific. Science 293 (5531), 847–849.